Supporting Information

Unlocking efficient near-infrared circularly polarized phosphorescence reaching 800 nm via rational molecular engineering of cyclometalated Pt(II) complexes

Shilin Gu,[†] Dongsheng Li,[†] Deng Long,[†] Xinglin Yu,[†] Wentao Li,*[,†] Sihan Ma,*[,†] and Peng Tao*[,‡]

[†]Institute of Advanced Optoelectronic Materials and Technology, College of Big Data and Information Engineering, Guizhou University, Guiyang 550025, P. R. China.

[‡]Department of Applied Biology and Chemical Technology and Research Institute for Smart Energy, The Hong Kong Polytechnic University, Hung Hom, Hong Kong, P. R. China; The Hong Kong Polytechnic University Shenzhen Research Institute, Shenzhen 518057, P. R. China.

*Corresponding Emails: wtli@gzu.edu.cn (Wentao Li); shma@gzu.edu.cn (Sihan Ma); pengtao@polyu.edu.hk (Peng Tao)

Materials and Methods

The information of the purchased chemicals used in this work.

Chemical	CAS No.	Purity	Supplier
1-chloroisoquinoline	19493-44-8	98%	Aladdin
4-fluorophenylboronic acid	214360-58-4	98%	Aladdin
1-chloroisoquinoline-4-carbonitrile	53491-80-8	98%	Aladdin
1-benzothiophen-2-ylboronic acid	98437-23-1	98%	Aladdin
$Pd(PPh_3)_4$	14221-01-3	99%	Aladdin
K_2PtCl_4	10025-99-7	98+%	Aladdin
(*R*)-4-phenyl-1,3-thiazolidine-2-thione	110199-18-3	98%	Aladdin
(*S*)-4-phenyl-1,3-thiazolidine-2-thione	185137-29-5	98%	Aladdin
ferrocene	102-54-5	98%	Aladdin
tetra-*n*-butylammonium hexafluorophosphate	3109-63-5	98%	Aladdin
CH_3CN	75-05-8	98%	Aladdin
ethyl acetate	141-78-6	98%	Shanghai Titan Scientific Co., Ltd.
n-hexane	110-54-3	98%	Shanghai Titan Scientific Co., Ltd.
K_2CO_3	584-08-7	99.5%	Shanghai Titan Scientific Co., Ltd.
Na_2SO_4	7757-82-6	99%	Shanghai Titan Scientific Co., Ltd.
2-ethoxyethanol	110-80-5	99%	Shanghai Titan Scientific Co., Ltd.
isopropanol	67-63-0	98%	Aladdin
diethyl ether	60-29-7	99.9+%	Aladdin
methanol	67-56-1	99.8+%	Bide Pharmatech Co., Ltd.
ethanol	64-17-5	99.5%	Aladdin
toluene	108-88-3	99.5%	Aladdin

The instrumental information used for characterizations in this work.

Characterization items	**Type**	**Manufacturer**
^{1}H, $^{13}C\{^{1}H\}$, and $^{19}F\{^{1}H\}$ NMR	AVANCE III HD, 400/600 MHz	Bruker, Germany
HRMS (ESI)	Agilent 6540 Quadrupole-TOF LC/MS	Agilent Technologies
Elemental analysis	VARIO EL cube	Elementar, Germany
UV-Vis absorption spectra	LAMBDA 950	Perkin Elmer USA
Photoluminescence spectra	FLS-1000	Edinburgh, USA
Photoluminescence quantum yield	FLS-1000	Edinburgh, USA
Lifetime	FLS-1000	Edinburgh, USA
CD spectra	CD *J*-1500	Jasco, Japan
Circularly polarized luminescence spectra	CPL-300	Jasco, Japan
CCD X-ray single crystal diffractometer	Bruker D8 VENTURE	Bruker, Germany
Electrochemical workstation	CHI600E	CH Instruments, China

General Experimental Details

Photophysical Measurements. The UV-Vis absorption spectra were recorded on a Perkin Elmer LAMBDA 950 UV-Vis spectrophotometer (Perkin Elmer, Waltham, MA, USA), and the optical HOMO–LUMO energy gaps of binuclear Pt(II) complexes **(*R*,*S*,*R*)/(*S*,*R*,*S*)-Pt1/Pt1** were calculated by the UV-Vis edge absorption (λ_{edge} = 629-774 nm). Steady-state emission experiments at room temperature were measured on an Edinburgh FLS-1000 spectrometer. Excited-state lifetime studies were performed with an Edinburgh FLS-1000 spectrometer with a hydrogen-filled excitation source. The data were analyzed by iterative convolution of the luminescence decay profile with the instrument response function using a software package provided by Edinburgh Instruments. Photoluminescence quantum yields (PLQY) of the complexes were determined through an absolute method by employing an integrating sphere. The solution was degassed by three freeze-pump-thaw cycles. Circular dichroism (CD) spectra were measured on a Jasco *J*-1500 circular dichroism spectrometer with a scan speed of 100 nm/min. The circularly polarized luminescence (CPL) spectra were measured on a Jasco CPL-300 spectrophotometer based on 'Continuous' scanning mode at 100 nm/min scan speed. The test mode adopts "Slit" mode with the Ex and Em slit width 2500 μm and the digital integration time (D.I.T.) is 2.0 s with multiple accumulations (10 times) and their $|g_{lum}|$ values were read from the curves recorded with the software bundled on the equipment.

X-ray Crystallographic Analysis. The single crystals of **(*R*,*S*,*R*)/(*S*,*R*,*S*)-Pt1/Pt2** were obtained from the solution mixture of dichloromethane and *n*-hexane. The X-ray diffraction data were collected on a Bruker Smart CCD Apex DUO diffractometer with graphite monochromated Mo K_α radiation (λ = 0.71073 Å) using the ω-2θ scan mode. The data were corrected for Lorenz and polarization effects. The structure was solved by direct methods and refined on F^2 by full-matrix least-squares methods using SHELXTL-2000.[1-3] All calculations and molecular graphics were carried out on a computer using the SHELX-2000 program package and Mercury. Crystallographic data for the structural analyses have been deposited with the Cambridge Crystallographic Data Center (CCDC). CCDC reference numbers for **(*R*,*S*,*R*)/(*S*,*R*,*S*)-Pt1/Pt2** are 2526096, 2526097, 2526098, and 2526099, respectively. Copies

of this information can be obtained free of charge from The Director, CCDC, 12 Union Road, Cambridge, CB2 1EZ, UK (Fax: +441223336033; E-mail: deposit@ccdc.cam.ac.uk, or www: http://www.ccdc.cam.ac.uk).

Electrochemical measurement. Cyclic voltammetry measurements were carried out in CH_3CN (5×10^{-4} M) with a three-electrode cell configuration consisting of platinum working and counter electrodes and a Ag/AgCl (0.01 M in CH_3CN) reference electrode at room temperature. Tetra-*n*-butylammonium hexafluorophosphate (Bu_4NPF_6, 0.1 M in CH_3CN) was used as the supporting electrolyte. The redox potentials were recorded at a scan rate of 100 mV/s and are reported with reference to the ferrocene/ferrocenium (Fc/Fc^+) redox couple. The energy levels were calculated using the following equations: $E_{HOMO} = -(E_{ox}^{1/2} - E_{Fc/Fc^+} + 4.8)$ eV,[4] $E_{LUMO} = E_{HOMO} + E_g^{opt}$, optical energy gap E_g^{opt} was estimated from the absorption onset using the equation ($E_g^{opt} = 1240/\lambda_{edge}$).[5]

Theoretical Calculations. To further interpret the UV-Vis spectral behavior of binuclear Pt(II) complexes **(*R*,*S*,*R*)/(*S*,*R*,*S*)-Pt1/Pt2**, the initial computational models of **(*R*,*S*,*R*)/(*S*,*R*,*S*)-Pt1/Pt2** were built according to their crystal structure. Their minimum energy structures based on the ground-state (S_0) were obtained from density functional theory (DFT) calculations which were carried out employing the popular B3LYP functional theory using ORCA software at the def2-TZVP[6] basis set with def2/J[7] and def2/JK[8] as auxiliary basis set. After that, their time-dependent DFT (TD-DFT) calculations were performed to explore energy transitions. The optimized structure of the ground-state (S_0) was used to calculate the UV-Vis absorption, PL, CD and CPL spectra by TD-DFT (dichloromethane as the solvent, pcm method, 100 singlet-singlet transitions and 100 singlet-triplet transitions). The luminescence dissymmetry factor g_{abs}/g_{lum} of a given transition (e.g., S_n (n = 1~4)/T_1 to S_0 (S_n (n = 1~4)/$T_1 \rightarrow S_0$)) is given by the equation $g_{abs}/g_{lum} = 4R/(D + G)$,[9] where $R = |\mu_e||\mu_m|\cos\theta$ is the transition rotatory strength, $D = |\mu_e|^2$ is the transition electric dipole strength, $G = |\mu_m|^2$ is the transition magnetic electric dipole strength, μ_e and μ_m are the electric and magnetic transition dipole moments, respectively, and θ the angle between the two. To compute g_{abs}/g_{lum}, the rotatory and dipole strength for the $S_0 \rightarrow S_n$ (n = 1~4)/$T_1 \rightarrow S_0$ transition from the S_n (n = 1~4)/T_1 state of binuclear Pt(II) complexes were

extracted from the ORCA output. The dipole strength is the square of the electric dipole moment as the length gauge, in au (1 au = 2.541746 D = 10^{-18} esu cm). From there, the g_{abs} and g_{lum} value can be computed at the wavelength of the transition.

Synthesis and Characterizations

Synthesis of H*C*^*N* ligand 1-(4-fluorophenyl)isoquinoline (F-Hpiq). The ligand **F-Hpiq** was synthesized from the improved Suzuki coupling reaction[10] of 1-chloroisoquinoline with 4-fluorophenylboronic acid. Tetrakis(triphenylphosphine)palladium (0) ($Pd(PPh_3)_4$, 0.347 g, 0.3 mmol) was added to a mixture of 1-chloroisoquinoline (1.080 g, 6.6 mmol), 4-fluorophenylboronic acid (0.840 g, 6 mmol), toluene (21 mL), ethanol (3 mL) and an aqueous potassium carbonate solution (2 M, 0.842 g in 6 mL water) under vigorous stirring. The mixture was stirred at 80 °C for 48 h under a nitrogen atmosphere. After cooling to room temperature, the reaction mixture was poured into water and extracted with ethyl acetate. The organic layer was washed with brine several times, and the solvent was then evaporated. Addition of CH_2Cl_2 followed by pentane precipitated a white solid which was filtered off. The residue was purified by column chromatography (SiO_2, *n*-Hexane/AcOEt, V/V = 8:1; R_f = 0.5) and isolated as a white solid. Yield: 1.044 g (78%). Anal calcd for $C_{15}H_{10}FN$: C, 80.70; H, 4.52; N, 6.27%. Found: C, 80.72; H, 4.48; N, 6.29%. ^{1}H NMR (600 MHz, $CDCl_3$, δ) 8.60 (d, J = 5.7 Hz, 1H), 8.07 (d, J = 8.5 Hz, 1H), 7.89 (d, J = 8.2 Hz, 1H), 7.75-7.63 (m, 4H), 7.56 (t, J = 7.7 Hz, 1H), 7.31-7.18 (m, 2H). ^{13}C{^{1}H} NMR (151 MHz, $CDCl_3$, δ) 163.24 (d, $^1J_{C\text{-}F}$ = 248.11 Hz), 159.77, 142.32, 137.04, 135.76 (d, $^4J_{C\text{-}F}$ = 3.29 Hz), 131.86 (d, $^3J_{C\text{-}F}$ = 8.24 Hz), 130.25, 130.25, 127.49, 127.32 (d, $^2J_{C\text{-}F}$ = 28.86 Hz), 126.80, 120.21, 115.59, 115.45, 115.43. ^{19}F{^{1}H} NMR (376.4 MHz, $CDCl_3$, δ) -113.15 (s). HRMS (ESI) (*m/z*): calcd for $C_{15}H_{10}FN+H^+$, 224.0870; found, 224.0595.

Synthesis of H*C*^*N* ligand 1-(benzo[*b*]thiophen-2-yl)isoquinoline-4-carbonitrile (CN-Hiqbt). The ligand **CN-Hiqbt** was obtained following a procedure analogous to that used for **F-Hpiq**. A mixture of 1-chloroisoquinoline-4-carbonitrile (0.623 g, 3.3 mmol), 1-benzothiophen-2-ylboronic acid (0.535 g, 3.0 mmol) was dissolved into absolute mixed solvents of toluene and EtOH (30 mL; V/V = 2:1) under an N_2 atmosphere. Then an aqueous solution (5 mL) of K_2CO_3

(2 M) was added, and the mixture was degassed by an N_2 flow. Anhydrous $Pd(PPh_3)_4$ (174 mg, 0.15 mmol) was added to the reaction mixture and then heated at 80 °C for 48 h. The complete consumption of reagents was monitored by thin-layer chromatography (*n*-Hexane/AcOEt, V:V = 5:1; R_f = 0.40). After cooling to room temperature, the organic phase was washed with brine and extracted with absolute CH_2Cl_2 (3×20 mL) three times. The combined organic phase was dried over anhydride Na_2SO_4, and further purified with flash-column chromatography on silica gel (*n*-Hexane/AcOEt, V/V = 5:1), affording to an off-white solid. Yield: 0.645 g (75%). Anal calcd for $C_{18}H_{10}N_2S$: C, 75.50; H, 3.52; N, 9.78%. Found: C, 75.53; H, 3.49; N, 9.74%. H NMR (600 MHz, $CDCl_3$, δ) 8.94 (s, 1H), 8.75 (d, J = 8.5 Hz, 1H), 8.31 – 8.26 (m, 1H), 7.98 – 7.94 (m, 3H), 7.93 – 7.91 (m, 1H), 7.83 (ddd, J = 8.3, 6.8, 1.2 Hz, 1H), 7.50 – 7.40 (m, 2H). $^{13}C\{^1H\}$ NMR (151 MHz, $CDCl_3$, δ) 157.55, 147.44, 141.66, 141.45, 140.03, 136.05, 132.85, 129.78, 127.90, 127.78, 126.27, 125.47, 125.06, 124.95, 122.59, 116.44, 104.81. HRMS (ESI) (*m/z*): calcd for $C_{18}H_{10}N_2S+H^+$, 287.0637; found, 286.9925.

Synthesis of the Pt(II) intermediates [Pt(F-piq)(F-Hpiq)Cl] and [Pt(CN-iqbt)(CN-Hiqbt)Cl]. K_2PtCl_4 (0.415 g, 1 mmol) and **F-Hpiq** (0.446 g, 2 mmol) in a 3:1 (V/V) mixture of 2-ethoxyethanol (18 mL) and H_2O (6 mL) were heated at 80 °C for 16 h under nitrogen atmosphere. After cooling to room temperature, saturated brine (30 mL) was added to the mixture. The precipitated yellow-green solid was collected by filtration and washed successively with isopropanol, diethyl ether, and hexane. The product was then dried under vacuum at 45 °C. The crude Pt(II) intermediate was directly used in the subsequent step without further purification. The Pt(II) intermediate **[Pt(CN-iqbt)(CN-Hiqbt)Cl]** was obtained by similar procedure.

Synthesis of the chiral binuclear Pt(II) complexes (*R*,*S*,*R*)/(*S*,*R*,*S*)-Pt1/Pt2. A mixture of the Pt(II) intermediate **[Pt(F-piq)(F-Hpiq)Cl]** or **[Pt(CN-iqbt)(CN-Hiqbt)Cl]**, (*R*)/(S)-4-phenyl-1,3-thiazolidine-2-thione (***R*/S-Hptt**), and K_2CO_3 (3 equiv.) in a sealed tube with dichloroethane was stirred at 80 °C for 24 h under an argon atmosphere. Then the solvent was removed under reduced pressure, and the residue of **(*R*,*S*,*R*)/(*S*,*R*,*S*)-Pt1/Pt2** was purified through column chromatography using petroleum ether and dichloromethane as the eluent to give the products

as powders.

(*R*,*S*,*R*)-Pt1. Deep-red solid (Yield: 32%): ^{1}H NMR (600 MHz, $CDCl_3$, δ) 8.13 (d, J = 8.6 Hz, 2H), 8.03 (d, J = 6.4 Hz, 2H), 7.70 (d, J = 8.2 Hz, 2H), 7.64 (d, J = 7.7 Hz, 4H), 7.60 (t, J = 7.4 Hz, 2H), 7.45 (t, J = 7.8 Hz, 2H), 7.23 (d, J = 6.4 Hz, 2H), 7.19 (dd, J = 8.7, 5.7 Hz, 2H), 7.09 (t, J = 7.5 Hz, 4H), 7.03 (t, J = 7.3 Hz, 2H), 6.86 (dd, J = 10.4, 2.7 Hz, 2H), 5.90 (t, J = 8.4 Hz, 2H), 5.79 (td, J = 8.5, 2.8 Hz, 2H), 3.95 (dd, J = 11.4, 8.4 Hz, 2H), 3.72 (dd, J = 11.4, 8.4 Hz, 2H). ^{13}C{^{1}H} NMR (151 MHz, $CDCl_3$, δ) 179.30, 165.20, 161.15 (d, $^{1}J_{C\text{-}F}$ = 254.10 Hz), 146.64 (d, $^{4}J_{C\text{-}F}$ = 6.63 Hz), 141.35, 140.26, 137.30, 130.69, 129.19 (d, $^{3}J_{C\text{-}F}$ = 8.79 Hz), 128.55, 128.53, 128.25, 127.27 (d, $^{3}J_{C\text{-}F}$ = 10.13 Hz), 126.58, 124.55, 119.87 (d, $^{2}J_{C\text{-}F}$ = 18.66 Hz), 119.07, 107.91 (d, $^{2}J_{C\text{-}F}$ = 22.92 Hz), 80.15, 41.90. ^{19}F{^{1}H} NMR (376.4 MHz, $CDCl_3$, δ) -110.87 (s), -110.87 (d, $^{4}J_{^{195}Pt\text{-}^{19}F}$ = 45.17 Hz). HRMS (ESI) (*m/z*): calcd for $C_{48}H_{34}F_2N_4Pt_2S_4$+$H^+$, 1223.0995; found, 1223.0996. Anal. calcd for $C_{48}H_{34}F_2N_4Pt_2S_4$: C, 47.13; H, 2.80; N, 4.58; found: C, 47.21; H, 2.81; N, 4.60.

(*S*,*R*,*S*)-Pt1. Deep-red solid (Yield: 35%): ^{1}H NMR (600 MHz, $CDCl_3$, δ) 8.13 (d, J = 8.6 Hz, 2H), 8.03 (d, J = 6.3 Hz, 2H), 7.70 (d, J = 8.2 Hz, 2H), 7.67 – 7.63 (m, 4H), 7.60 (t, J = 7.4 Hz, 2H), 7.48 – 7.42 (m, 2H), 7.23 (d, J = 6.4 Hz, 2H), 7.19 (dd, J = 8.6, 5.7 Hz, 2H), 7.09 (t, J = 7.5 Hz, 4H), 7.03 (t, J = 7.3 Hz, 2H), 6.86 (dd, J = 10.3, 2.7 Hz, 2H), 5.90 (t, J = 8.4 Hz, 2H), 5.79 (td, J = 8.5, 2.8 Hz, 2H), 3.95 (dd, J = 11.4, 8.4 Hz, 2H), 3.72 (dd, J = 11.4, 8.4 Hz, 2H). ^{13}C{^{1}H} NMR (151 MHz, $CDCl_3$, δ) 179.30, 165.20, 161.15 (d, $^{1}J_{C\text{-}F}$ = 254.10 Hz), 146.64 (d, $^{4}J_{C\text{-}F}$ = 6.63 Hz), 141.35, 140.26, 137.30, 130.69, 129.19 (d, $^{3}J_{C\text{-}F}$ = 8.79 Hz), 128.55, 128.53, 128.25, 127.27 (d, $^{3}J_{C\text{-}F}$ = 10.13 Hz), 126.58, 124.55, 119.87 (d, $^{2}J_{C\text{-}F}$ = 18.66 Hz), 119.07, 107.91 (d, $^{2}J_{C\text{-}F}$ = 22.92 Hz), 80.15, 41.90. ^{19}F{^{1}H} NMR (376.4 MHz, $CDCl_3$, δ) -110.88 (s), -110.87 (d, $^{4}J_{^{195}Pt\text{-}^{19}F}$ = 45.17 Hz). HRMS (ESI) (*m/z*): calcd for $C_{48}H_{34}F_2N_4Pt_2S_4$+$H^+$, 1223.0995; found, 1223.0994. Anal. calcd for $C_{48}H_{34}F_2N_4Pt_2S_4$: C, 47.13; H, 2.80; N, 4.58; found: C, 47.17; H, 2.84; N, 4.60.

(*R*,*S*,*R*)-Pt2. Dark maroon solid (Yield: 28%): ^{1}H NMR (600 MHz, $CDCl_3$, δ) 8.76 (d, J = 8.1 Hz, 2H), 8.44 (d, J = 8.3 Hz, 2H), 7.82 (s, 2H), 7.80 – 7.73 (m, 4H), 7.63 – 7.51 (m, 6H), 7.19 (dd, J = 8.6, 6.8 Hz, 6H), 7.12 – 7.06 (m, 2H), 6.86 – 6.77 (m, 4H), 6.16 (dd, J = 9.1, 5.4 Hz,

2H), 4.23 (dd, J = 11.5, 9.1 Hz, 2H), 3.90 (dd, J = 11.5, 5.5 Hz, 2H). $^{13}C\{^{1}H\}$ NMR (151 MHz, $CDCl_3$, δ) 180.20, 165.00, 154.54, 146.92, 143.92, 143.64, 139.95, 137.71, 134.88, 132.82, 129.79, 129.25, 128.87, 128.37, 128.23, 128.12, 127.04, 124.33, 123.83, 122.51, 120.38, 116.11, 100.95, 79.72, 41.49. HRMS (ESI) (*m/z*): calcd for $C_{54}H_{34}N_6Pt_2S_6+H^+$, 1350.0539; found, 1350.0536. Anal. calcd for $C_{54}H_{34}N_6Pt_2S_6$: C, 48.06; H, 2.54; N, 6.23; found: C, 48.04; H, 2.49; N, 6.19.

(*S*,*R*,*S*)-Pt2. Dark maroon solid (Yield: 30%): ^{1}H NMR (600 MHz, $CDCl_3$, δ) 8.76 (d, J = 8.2 Hz, 2H), 8.44 (dd, J = 8.1, 1.6 Hz, 2H), 7.82 (s, 2H), 7.80 – 7.74 (m, 4H), 7.58 – 7.53 (m, 6H), 7.22 – 7.14 (m, 6H), 7.13 – 7.06 (m, 2H), 6.87 – 6.78 (m, 4H), 6.16 (dd, J = 9.1, 5.4 Hz, 2H), 4.23 (dd, J = 11.5, 9.1 Hz, 2H), 3.90 (dd, J = 11.5, 5.4 Hz, 2H). $^{13}C\{^{1}H\}$ NMR (151 MHz, $CDCl_3$, δ) 180.20, 167.89, 165.00, 154.54, 146.92, 143.92, 143.63, 139.94, 137.71, 134.88, 132.82, 132.45, 131.08, 129.79, 129.25, 129.00, 128.87, 128.38, 128.22, 128.12, 127.04, 124.34, 123.83, 122.50, 120.38, 116.11, 100.95, 79.72, 41.49. HRMS (ESI) (*m/z*): calcd for $C_{54}H_{34}N_6Pt_2S_6+H^+$, 1350.0539; found, 1350.0541. Anal. calcd for $C_{54}H_{34}N_6Pt_2S_6$: C, 48.06; H, 2.54; N, 6.23; found: C, 48.07; H, 2.56; N, 6.17.

Scheme S1. Chemical structures and synthetic routes of the chiral binuclear Pt(II) complexes**.**

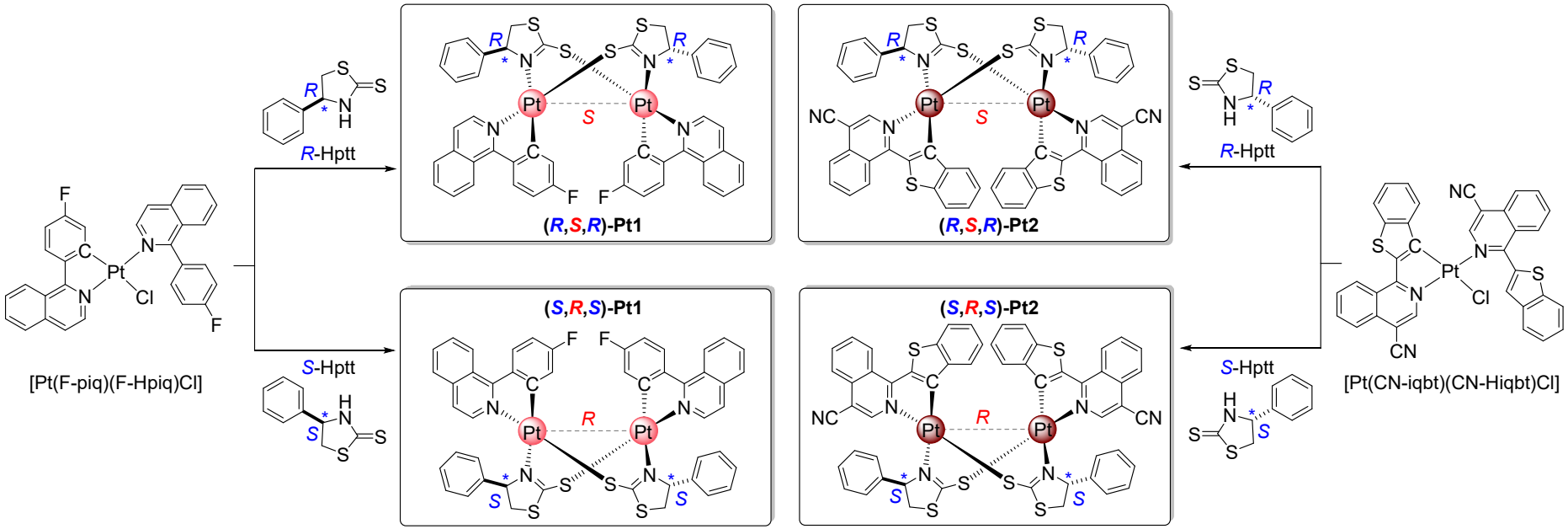

Table S1. The selected ^{1}H NMR data for the chiral binuclear Pt(II) complexes.

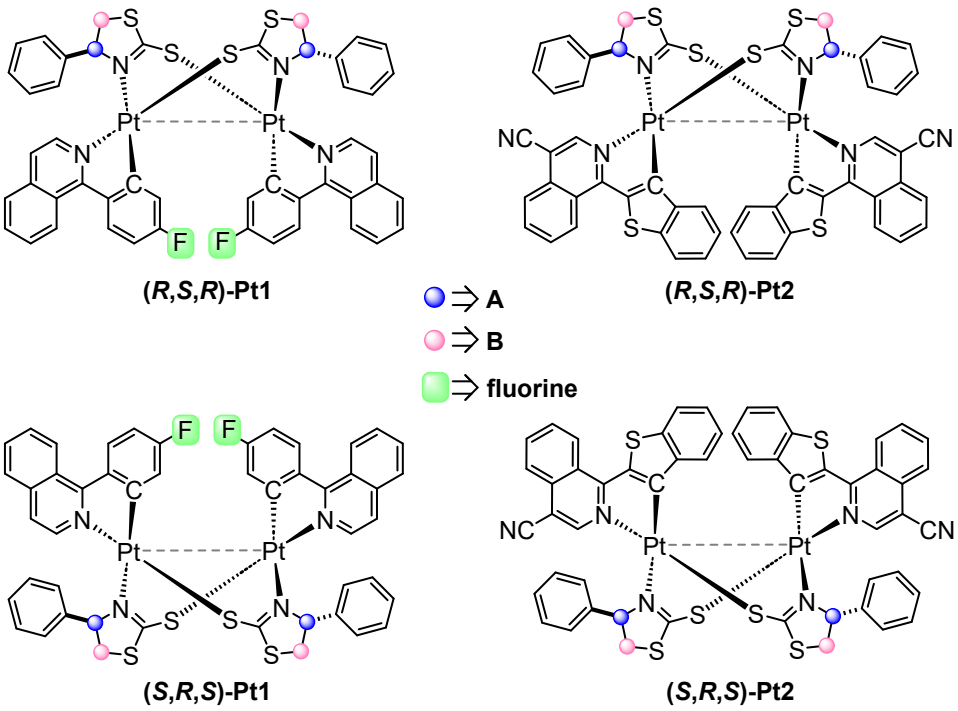

Complex	Chemical shift (ppm)						
	The combined proton resonances	H_A	H_B	The combined carbon resonances	C_A	C_B	The fluorine resonances
(*R*,*S*,*R*)-Pt1	8.13-3.72	5.79	3.75, 3.72	179.30-41.90	80.15	41.90	-110.87
(*S*,*R*,*S*)-Pt1	8.13-3.72	5.79	3.75, 3.72	179.30-41.90	80.15	41.90	-110.88
(*R*,*S*,*R*)-Pt2	8.76-3.90	6.16	4.23, 3.90	180.20-41.49	79.72	41.49	/
(*S*,*R*,*S*)-Pt2	8.76-3.90	6.16	4.23, 3.90	180.20-41.49	79.72	41.49	/

[a)]All ^{1}H NMR, ^{13}C{^{1}H} NMR and ^{19}F{^{1}H} NMR spectra were recorded in $CDCl_3$ at room temperature.

Table S2. Selected crystallographic data for the chiral binuclear Pt(II) complexes.

Complex	(*R*,*S*,*R*)-Pt1	(*S*,*R*,*S*)-Pt1	(*R*,*S*,*R*)-Pt2	(*S*,*R*,*S*)-Pt2
Chemical formula	$C_{48}H_{34}F_2N_4Pt_2S_4$	$C_{48}H_{34}F_2N_4Pt_2S_4$	$C_{54}H_{34}N_6Pt_2S_6$	$C_{54}H_{34}N_6Pt_2S_6$
CCDC number	2526096	2526097	2526098	2526099
Crystal size (mm)	0.20 × 0.20 × 0.18	0.21 × 0.20 × 0.17	0.20 × 0.18 × 0.20	0.20 × 0.20 × 0.18
Temperature/K	193	150	150	200
Crystal system	monoclinic	monoclinic	orthorhombic	orthorhombic
Space group	$P2_1$	$P2_1$	$P2_12_12_1$	$P2_12_12_1$
a/Å	11.3739(10)	11.2864(5)	12.5446(9)	12.6435(11)
b/Å	15.5577(12)	15.3857(6)	19.2471(15)	19.402(2)
c/Å	12.1253(11)	12.0821(6)	22.0945(18)	22.375(3)
α/°	90	90	90	90
β/°	98.352(3)	98.285(2)	90	90
γ/°	90	90	90	90
V/Å^3	2122.8(3)	2076.15(16)	5334.7(7)	5489.0(10)
Z	2	2	4	4
ρ_{calc} (g/cm^3)	1.914	1.957	1.680	1.838
μ/mm^{-1}	6.829	6.982	5.515	5.559
F(000)	1176.0	1176.0	2608.0	2944.0
Reflections collected	20000	96796	189858	23637
GOF (F^2)	1.062	1.017	0.979	1.005
R_{int}	0.0601	0.0532	0.0811	0.0359
R_{sigma}	0.0686	0.0304	0.0314	0.0672
R_1/wR_2 [$I>=2\sigma(I)$]	0.0444/0.1140	0.0146/0.0285	0.0242/0.0626	0.0362/0.0839
R_1/wR_2 [all data]	0.0497/0.1188	0.0159/0.0288	0.0255/0.0632	0.0449/0.0877
Flack parameter	0.074(17)	0.008(2)	0.067(5)	0.090(9)

Table S3. The selected bond lengths (Å) and bond angles (°) for the chiral binuclear Pt(II) complexes.

Complex	(*R*,*S*,*R*)-Pt1	(*S*,*R*,*S*)-Pt1	Complex	(*R*,*S*,*R*)-Pt2	(*S*,*R*,*S*)-Pt2
Selected bond	Bond length (Å)		Selected bond	Bond length (Å)	
Pt(1)-N(1)	2.158(14)	2.151(3)	Pt(1)-N(1)	2.123(4)	2.134(7)
Pt(1)-N(3)	2.050(15)	2.037(3)	Pt(1)-N(3)	2.072(5)	2.086(7)
Pt(1)-S(2)	2.299(5)	2.291(10)	Pt(1)-S(2)	2.295(14)	2.303(2)
Pt(1)-C(29)	2.021(8)	1.982(4)	Pt(1)-C(29)	1.993(5)	2.008(8)
Pt(2)-N(2)	2.105(13)	2.140(3)	Pt(2)-N(2)	2.127(5)	2.168(8)
Pt(2)-N(4)	2.053(11)	2.049(3)	Pt(2)-N(4)	2.066(5)	2.055(8)
Pt(2)-S(1)	2.286(4)	2.2821(8)	Pt(2)-S(1)	2.290(15)	2.290(3)
Pt(2)-C(44)	2.013(7)	1.980(3)	Pt(2)-C(47)	1.991(6)	2.015(9)
Selected bond angle	Bond angles (°)		Selected bond angle	Bond angles (°)	
C(29)-Pt(1)-N(1)	176.7(5)	176.69(15)	C(29)-Pt(1)-N(1)	174.7(2)	174.9(4)
C(29)-Pt(1)-N(3)	79.7(5)	80.17(15)	C(29)-Pt(1)-N(3)	79.9(2)	79.9(3)
N(1)-Pt(1)-S(2)	87.1(4)	87.97(9)	N(1)-Pt(1)-S(2)	85.65(15)	85.5(2)
N(3)-Pt(1)-S(2)	175.2(4)	174.88(9)	N(3)-Pt(1)-S(2)	79.18(16)	179.4(2)
C(44)-Pt(2)-N(2)	176.8(5)	177.85(13)	C(47)-Pt(2)-N(2)	175.9(2)	175.1(3)
C(44)-Pt(2)-N(4)	79.8(5)	80.27(12)	C(47)-Pt(2)-N(4)	80.1(2)	79.8(3)
N(2)-Pt(2)-S(1)	86.9(4)	86.75(8)	N(2)-Pt(2)-S(1)	86.18(13)	86.6(2)
N(4)-Pt(2)-S(1)	174.9(4)	174.76(8)	N(4)-Pt(2)-S(1)	177.65(16)	178.0(2)

Table S4. Intramolecular Pt-Pt distances, intermolecular noncovalent interactions and intermolecular π-π interactions between molecules for the chiral binuclear Pt(II) complexes.

Complex	Intramolecular Pt-Pt distances (Å)	Intermolecular noncovalent interactions (Å)		Intermolecular π-π interactions between molecules (Å)
(*R*,*S*,*R*)-Pt1	2.922	S···H	2.970, 2.931	3.395
		F···H	2.617, 2.647, 2.609	
(*S*,*R*,*S*)-Pt1	2.910	S···H	3.343, 2.872	3.370
		F···H	2.603, 2.527, 2.617	
(*R*,*S*,*R*)-Pt2	2.941	S···H	2.818, 2.999	3.422
		F···H	2.396	
(*S*,*R*,*S*)-Pt2	2.948	S···H	2.919	3.417
		F···H	2.518	

Table S5. Photophysical properties of the chiral binuclear Pt(II) complexes at room temperature.

Complex	Medium	Absorption	Emission					
		λ_{abs} (ε [× 10^3 M^{-1} cm^{-1}]) [λ_{edge}^{onset}] (nm)	λ_{PL}[a] (nm)	τ[a] (μs)	PLQY[a] (%)	g_{lum}[b] (10^{-3})	B_{CPL}[c] (M^{-1} cm^{-1})	E_g^{opt}[d] (eV)
(*R*,*S*,*R*)-Pt1	CH_2Cl_2	228 (60.4), 272 (40.1), 350 (11.5), 383 (8.5), 416 (4.8), 523 (2.7), 546 (2.6) [629][e]	733[e]	0.35[e]	20.6[e]	-2.5[f]	0.7[f]	1.97
	Doped film	-	709[g]	1.83[g]	35.4[g]	-2.8[h]	-	-
(*S*,*R*,*S*)-Pt1	CH_2Cl_2	225 (56.8), 272 (36.7), 350 (10.5), 382 (7.8), 416 (4.4), 521 (2.4), 546 (2.4) [629][e]	731[e]	0.40[e]	21.0[e]	+2.5[f]	0.6[f]	1.97
	Doped film	-	708[g]	1.84[g]	34.2[g]	+2.7[h]	-	-
(*R*,*S*,*R*)-Pt2	CH_2Cl_2	236 (54.3), 319 (22.6), 412 (12.1), 472 (11.2), 542 (8.9), 616 (4.3) [774][e]	780, 835(sh)[e]	0.35[e]	18.9[e]	-2.1[f]	0.9[f]	1.60
	Doped film	-	792[g]	1.25[g]	29.2[g]	-3.9[h]	-	-
(*S*,*R*,*S*)-Pt2	CH_2Cl_2	236 (56.8), 330 (22.5), 412 (12.6), 473 (11.8), 541 (9.2), 613 (4.4) [774][e]	775, 837(sh)[e]	0.32[e]	17.8[e]	+2.1[f]	0.8[f]	1.60
	Doped film	-	794[g]	1.29[g]	28.5[g]	+3.8[h]	-	-

[a]Excitation wavelength 375 nm; [b]at Wavelength of the PL maximum (λ_{PL}^{Max}), [c]CPL brightness (B_{CPL}) were defined as the following equation $B_{CPL} = \varepsilon_\lambda \times$ PLQY $\times |g_{lum}|/2$, [d]$E_g^{opt} = 1240/\lambda_{edge}^{onset}$; [e]At 1.0 × 10^{-5} mol/L in degassed CH_2Cl_2; [f] At 0.5 × 10^{-5} mol/L in degassed CH_2Cl_2; [g]The complex was doped in poly(methyl methacrylate (PMMA) film (5 wt%); [h]The complex was doped in poly(methyl methacrylate (PMMA) film (2 wt%).

Table S6. Excitation wavelengths (nm), oscillator strengths (*f*) and the corresponding transition and properties for the chiral binuclear Pt(II) complexes.

Complex	State	λ (nm)	E (eV)	Oscillator (*f*)	Orbital contribution (>5%)
(*R*,*S*,*R*)-Pt1	$S_0 \rightarrow T_1$	1056	1.17	0.0082	HOMO→LUMO (93.9%)
	$S_0 \rightarrow S_1$	895	1.39	0.0241	HOMO→LUMO (99.3%)
(*S*,*R*,*S*)-Pt1	$S_0 \rightarrow T_1$	1056	1.17	0.0083	HOMO→LUMO (94.0%)
	$S_0 \rightarrow S_1$	895	1.39	0.0242	HOMO→LUMO (99.3%)
(*R*,*S*,*R*)-Pt2	$S_0 \rightarrow T_1$	1226	1.01	0.0002	HOMO→LUMO (94.3%)
	$S_0 \rightarrow S_1$	986	1.26	0.0298	HOMO → LUMO (99.3%)
(*S*,*R*,*S*)-Pt2	$S_0 \rightarrow T_1$	1216	1.02	0.0001	HOMO → LUMO (94.2%)
	$S_0 \rightarrow S_1$	978	1.27	0.0301	HOMO → LUMO (99.3%)

Table S7. Frontier orbitals and their corresponding electron cloud density distributions for the chiral binuclear Pt(II) complexes.

Complex	Orbital	Contribution of metal d_π orbitals and π orbitals of ligand to MOs (%)		
		Pt	**F-piq**	***R/S*-ptt**
(*R*,*S*,*R*)-Pt1	LUMO	6.18	92.00	1.82
	HOMO	78.97	11.70	9.33
(*S*,*R*,*S*)-Pt1	LUMO	6.00	92.25	1.75
	HOMO	79.10	11.39	9.51
	Orbital	**Pt**	**CN-iqbt**	***R/S*-ptt**
(*R*,*S*,*R*)-Pt2	LUMO	7.27	90.77	1.96
	HOMO	73.77	17.05	9.18
(*S*,*R*,*S*)-Pt2	LUMO	7.02	91.17	1.82
	HOMO	75.69	14.99	9.32

Table S8. Voltammetric data for the chiral binuclear Pt(II) complexes.

Complex	$E_{ox}^{1/2}$ (V)[a]	E_{HOMO} (eV)[b]	λ_{edge}^{onset} (nm)	E_g^{opt} (eV)[c]	E_{LUMO} (eV)[d]
(*R*,*S*,*R*)-Pt1	0.61	-4.90	629	1.97	-2.93
(*S*,*R*,*S*)-Pt1	0.60	-4.89	629	1.97	-2.92
(*R*,*S*,*R*)-Pt2	0.89	-5.18	774	1.60	-3.58
(*S*,*R*,*S*)-Pt2	0.88	-5.17	774	1.60	-3.57

[a]Reversible. The values were derived from the anodic peak potential. [b]HOMO levels are calculated from the equation ($E_{HOMO} = -(E_{ox}^{1/2} - E_{Fc/Fc^+} + 4.8)$ eV; where $E_{ox}^{1/2}$ is measured in CH_2Cl_2 and reported *versus* the Ag/AgCl). [c]Optical energy gap E_g^{opt} was estimated from the absorption onset using the equation ($E_g^{opt} = 1240/\lambda_{edge}^{onset}$). [d]The LUMO energy levels of each complex were calculated according to the following equation ($E_{LUMO} = E_{HOMO} + E_g^{opt}$). Note: $E_{Fc/Fc^+} = 0.51$ V.

Table S9. Calculated transition dipole moments and chiroptical properties for the chiral binuclear Pt(II) complexes based on optimized S_0 geometries.

Complex	State	E (eV)	$\lvert\boldsymbol{\mu}_e\rvert$[a] ($\times10^{-20}$ esu·cm)	$\lvert\boldsymbol{\mu}_m\rvert$[b] ($\times10^{-18}$ erg·G^{-1})	$\theta_{e,m}$[c] (°)	g_{abs}[d] ($\times10^{-2}$)
***(R,S,R)*-Pt1**	S_1	1.39	21.5	8.7	14.9	-0.3
	S_2	1.73	11.3	6.5	137.2	0.3
	S_3	2.40	36.9	25.6	109.1	1.8
	S_4	2.43	34.2	22.3	150.1	4.5
***(S,R,S)*-Pt1**	S_1	1.39	84.6	9.4	163.1	0.3
	S_2	1.74	45.1	7.3	43.4	-0.3
	S_3	2.39	12.6	25.5	71.7	-1.8
	S_4	2.43	14.3	22.8	22.9	-4.2
***(R,S,R)*-Pt2**	S_1	1.26	97.4	9.8	9.9	-0.3
	S_2	1.59	49.7	1.8	21.6	-0.1
	S_3	1.89	25.4	43.1	177.1	4.9
	S_4	2.10	51.1	45.7	68.6	-0.9
***(S,R,S)*-Pt2**	S_1	1.27	97.6	9.5	170.1	0.3
	S_2	1.59	50.1	1.4	170.6	0.1
	S_3	1.89	23.8	43.2	1.4	-5.3
	S_4	2.10	51.3	45.4	111.9	0.9

[a]Transition electric dipole moment (TEDM). [b]Transition magnetic dipole moment (TMDM). [c]$\theta_{e,m}$ represents the angle of TEDM and TMDM. [d]Absorption asymmetry g-factors (g_{abs}) is calculated as follows: $g_{abs} = 4R/(D + G)$, where R, D, and G represent the rotatory, electric dipole, and magnetic dipole strength, respectively ($R = |\mu_e||\mu_m|\cos\theta$, $D = |\mu_e|^2$, $G = |\mu_m|^2$).

Table S10. Calculated transition dipole moments and chiroptical properties for the chiral binuclear Pt(II) complexes based on optimized T_1 geometries.

Complex	State	E (eV)	$\|\boldsymbol{\mu}_e\|$[a] ($\times10^{-20}$ esu·cm)	$\|\boldsymbol{\mu}_m\|$[b] ($\times10^{-22}$ erg·G^{-1})	$\theta_{e,m}$[c] (°)	g_{lum}[d] ($\times10^{-3}$)
(*R*,*S*,*R*)-Pt1	T_1	1.24	3.9	0.6	45.4	3.3
(*S*,*R*,*S*)-Pt1		1.24	3.9	0.7	44.2	-3.4
(*R*,*S*,*R*)-Pt2		1.08	2.9	0.2	2.4	1.8
(*S*,*R*,*S*)-Pt2		1.09	3.0	0.2	0.4	-1.6

[a]Transition electric dipole moment (TEDM). [b]Transition magnetic dipole moment (TMDM). [c]$\theta_{e,m}$ represents the angle of TEDM and TMDM. [d]Luminescence asymmetry *g*-factors (g_{lum}) is calculated as follows: $g_{lum} = 4R/(D + G)$, where R, D, and G represent the rotatory, electric dipole, and magnetic dipole strength, respectively ($R = |\mu_e||\mu_m|\cos\theta$, $D = |\mu_e|^2$, $G = |\mu_m|^2$).

Table S11. Comparison of PLQYs of the designed Pt(II) complexes with the reported Ir(III) and Pt(II) complexes showing PL at NIR region.

Complex	λ_{PL} (nm)	PLQY	Ref.
The reported near-infrared photoluminescent dinuclear Pt(II) complexes			
5	706	0.36	*Angew. Chem. Int. Ed.* 2026, **65**, e19762
7	702	0.64	
4b	794	0.3	*J Korean Chem Soc*, 2025, **69**, 39
[Pt(tfppy)(*μ*-PyXZ)] (2)	705	0.46	*Adv. Optical Mater.,* 2023, **11**, 2300201
[Pt(piq)(*μ*-Czl)] (Pt-4)	740	0.29	*Mater. Chem. Front.,* 2023, **7**, 873
1	726	0.11	*Adv. Funct. Mater.,* 2023, **33**, 2211853
2	712	0.16	
3	722	0.18	
4	701	0.17	
1	706	0.16	*Inorg. Chem.,* 2022, **61**, 121
2	725	0.095	
3	736	0.083	
4	710	0.013	
5	725	0.104	
Pt-4	802	0.05	*Inorg. Chem.,* 2022, **61**, 5178
Pt-5	758	0.07	
Pt_2(bis-dthpym)$(dpm)_2$	725	0.17	*J. Mater. Chem. C*, 2021, **9**, 127
(DIQB)$[Pt(DPM)]_2$	730	0.0077	*Org. Electron.*, 2020, **87**, 105902
(BuPh-BDIQ)$Pt_2(dpm)_2$	718	0.0364	*J. Mater. Chem. C*, 2018, **6**, 5769
1	726	0.0397	*Inorg. Chem.,* 2018, **57**, 1298

2	738	0.0188	
3	766	0.0051	
4	777	0.033	
4	744	0.062	*Dyes Pigment.,* 2017, **145**, 144
7	745	0.046	
$(piq)_2Pt_2(\mu$-PhOXT$)_2$	702	0.315	*J. Mater. Chem. C*, 2016, **4**, 6007
$(piq)_2Pt_2(\mu$-C_8PhOXT$)_2$	703	0.295	
(piq)Pt(μ-C_8OXT)$_2$Pt(piq)	721	0.18	*Org. Electron.*, 2012, **13**, 932
4	715	0.0005	*Bull. Chem. Soc. Jpn.,* 2011, **84**, 219
(*R*,*S*,*R*)-Pt1	733	0.206	**This work**
(*S*,*R*,*S*)-Pt1	731	0.210	
(*R*,*S*,*R*)-Pt2	780	0.189	
(*S*,*R*,*S*)-Pt2	775	0.178	
The reported near-infrared photoluminescent Ir(III) complexes			
IrFTIQ	738	0.085	*Dyes Pigment.,* 2025, **232**, 112500
Ir(Bpiq)$_2$acac	722	0.35	*Chin. Chem. Lett.*, 2025, 36, 109596
Ir(Bpiq)$_2$dpm	728	0.33	
(Epptt)$_2$Iracac (1)	756	0.124	*Adv. Optical Mater.,* 2025, **13**, 2402178
(pptt)$_2$Iracac (2)	796	0.078	
(ppCz)$_2$Irtmd (3)	862	0.006	
[Ir(dpbq)$_2$(pbi))] (1)	783	0.034	*J. Mater. Chem. C*, 2025,**13**, 7110
[Ir(dpbq)(iqbt)(pbi)] (2)	791	0.042	
[Ir(iqbt)(pbao)(acac)] (2)	719	0.023	*J. Lumin.*, 2025, **288**, 121550

[Ir(dpbq)$_2$(L^1)] (1)	787	0.022	*J. Lumin.,* 2024, **269**, 120487
[Ir(dpbq)$_2$(L^2)] (2)	784	0.036	
TPAIr	774	0.15	
HTIr	788	0.09	*Chem. Eng. J.*, 2023, **452**, 138956
DPTAIr	798	0.11	
DTCNIr	722	0.15	*Adv. Optical Mater.*, 2022, **10**, 2200111
PTCNIr	750	0.26	
BiqThIr	731	0.68	*Angew. Chem. Int. Ed.*, 2023, **62**, e202309739
BiqThIrO	728	0.70	
DBPzIr	746	0.40	*Dalton Trans.*, 2023, **52**, 16276
PPzIr	789	0.14	
1	712	0.29	*J. Mater. Chem. C,* 2022, **10**, 3178
2	714	0.36	
Ir(dotbpa)$_3$	839	0.015	*J. Mater. Chem. C,* 2020, **8**, 8484
Ir1	712	0.18	*Adv. Optical Mater.*, 2020, **8**, 2000154
Ir2	741	0.2	
Ir3	716	0.25	
Ir4	728	0.3	
TCNIr	708	0.06	*Chem. Sci*., 2020, **11**, 2342
Ir-R	732	0.28	*J. Mater. Chem. C*, 2020, **8**, 7079
Ir-OR	775	0.08	
(PPz-11,12-DO)$_2$Iracac	732	0.13	*J. Mater. Chem. C*, 2019, **7**, 10961
[(iqbt)$_2$Ir-(btp)-Ir(iqbt)$_2$]	722	0.15	*J. Lumin.*, 2019, **209**, 427

Ir-3	758	0.011	*J. Mater. Chem. C*, 2018, **6**, 10640
Ir-4	722	0.106	
***fac*-Ir(dtbpa)$_3$ (1)**	824	0.029	*Chem. Mater.*, 2017, **29**, 4775
***fac*-Ir(Ftbpa)$_3$ (2)**	765	0.147	
[Ir(iqbt)$_2$(dpm)] (1)	710	0.16	
[Ir(iqbt)$_2$(tta)] (2)	704	0.07	*Angew. Chem. Int. Ed.*, 2016, **55**, 2714
[Ir(iqbt)$_2$(dtdk)] (3)	707	0.14	
(thdpqx)$_2$Ir(acac)	713	0.149	*Chem. Mater.*, 2015, **27**, 96

Table S12. Summary of photophysical properties for the chiral Pt(II) complexes.

Complex	λ_{PL} (nm)	PLQY	$g_{lum}(10^{-3})$	Ref.
***R*-$PtCl_2$**	660	0.357	4.0	*Inorg. Chim. Acta*, 2025, **579**, 122589
(*D*,*R*,*D*)/(*L*,*S*,*L*)-[(L1)(L2)Pt_2(μ-itt)$_2$]	624	0.127	0.87/-1.02	
(*D*,*R*,*D*)/(*L*,*S*,*L*)-[(L2)(L3)Pt_2(μ-itt)$_2$]	666	0.036	1.68/-2.23	
(*D*,*R*,*D*)/(*L*,*S*,*L*)-[(L1)$_2$$Pt_2$($\mu$-itt)$_2$]	622	0.198	2.58/-2.62	*Org. Lett.*, 2025, **27**, 6971
(*D*,*R*,*D*)/(*L*,*S*,*L*)-[(L2)$_2$$Pt_2$($\mu$-itt)$_2$]	616	0.114	1.36/-2.12	
(*D*,*R*,*D*)/(*L*,*S*,*L*)-[(L3)$_2$$Pt_2$($\mu$-itt)$_2$]	694	0.024	1.68/-1.70	
R*,*R*/*S*,*S	~615	0.003	±2.5	Chem. Lett., 2025, **54**, upaf140
L-Pt	580	0.53	0.40	*Angew. Chem. Int. Ed.*, 2024, **63**, e202403898
(*R*)/(*S*)-OMOM-Me	660	0.302	1.00/-0.92	
(*R*)/(*S*)-OAc- Me	656	0.315	1.31/-1.32	*Sci. China Chem.*, 2024, **67**, 3757
(*R*)/(*S*)-OMe -Me	665	0.295	1.30/-1.20	
***R*-ABA·[Pt(ppy)Cl_2]**	521	0.199	1.40	
***S*-ABA·[Pt(ppy)Cl_2]**	520	0.196	-1.80	*Mater. Horiz.,* 2024, **11**, 6089
***R*-MBA·[Pt(ppy)Cl_2]**	522	0.133	4.40	
***S*-MBA·[Pt(ppy)Cl_2]**	523	0.132	-2.80	
12a	~515		5.0	*Acc. Chem. Res.*, 2024, **57**, 2941
12b	~515		2.0	
(S)-1a	508	0.02	3.0	
(S)-1b	512	0.04	2.0	*Inorg. Chem.*, 2024, **63**, 23642
(S)-1c	518	0.03	3.0	
(S)-2a	555	＜0.01	-	

(S)-2b	550	＜0.01	-	
(S)-2c	530	＜0.01	-	
***(R,R,R,R$_p$,M)/(S,S,S,S$_p$,P)*-Me**	635	0.062	−0.67/0.67	*Inorg. Chem.*, 2023, **62**, 14152
***(R,R,R,R$_p$,M)/(S,S,S,S$_p$,P)*-iPr**	635	0.066	−1.09/0.89	
***R*-Pt**	621	0.0046	3.4	*Chem. Commun.,* 2023, **59**, 4004
S-Pt	621	0.0055	-2.3	
(*L,S,L*)Pt4a	622	0.198	-1.21	*Angew. Chem. Int. Ed.*, 2023, **62**, e202302011
(*L,S,L*)Pt4b	617	0.215	-4.13	
1	520	0.05	0.67	*ChemPhotoChem*, 2023, **7**, e202300010
***(RR)(SS)*-Py-Pt**	~550	0.0672	-0.77/0.63	*Chin. Chem. Lett.*, 2022, **33**, 1459
***(RR)(SS)-P/M*-QPt**	~634	0.0199	-3.5/3.1	
***(R)*-Cy-A**	605	0.152	2.0	
***(R,R,R)*-BINA-A**	520	0.342	2.4	*J. Am. Chem. Soc.*, 2022, **144**, 2233
***(R,R,R)*-BINA-B**	718	0.081	1.0	
***trans*-[Pt(ppy)(D-tac)]**	521	-	＜0.2	*Inorg. Chem.*, 2022, **61**, 17154
***cis*-[Pt(ppy)(D-tac)]**	521	-	＜0.2	
***trans*-[Pt(ppy)(D-pbc)]**	518	-	＜0.2	
***cis*-[Pt(ppy)(D-pbc)]**	550	-	＜0.2	
(*S,S*)-1	533	0.10	1.0	*Chem. Lett.* 2022, **51**, 832
(*S,S*)-2	575	0.05	0.8	
***R*-NCN**	523	0.200	0.10	*J. Organomet. Chem.*, 2022, **973-974**, 122394.
***S*-NCN**	523	0.196	0.10	
Phen-NCN	530	0.224	0.10	

***P*-Pt**	650	-	-6.0	*Front. Chem*., 2020, **8**, 501
***M*-Pt**	650	-	6.0	
(*R*)/(*S*)-BP1	645	0.32	±1.3	*ACS Appl. Mater. Interfaces*, 2020, **12**, 9520
(*R*)/(*S*)-BP2	639	0.12	±1.0	
[Pt(iqbt)(*S*-L^1)] (1)	731	0.13	-2.14	
[Pt(iqbt)(*S*-L^2)] (2)	729	0.21	2.04	*J. Mater. Chem. C*, 2019, **7**, 13743
[Pt(iqbt)(*S*-L^2)] (3)	730	0.16	-1.76	
[Pt(iqbt)(*S*-L^2)] (4)	731	0.14	-2.75	
(*R*,*S*,*R*)-Pt1	709	0.354	-2.8	**This work**
(*S*,*R*,*S*)-Pt1	708	0.342	2.7	
(*R*,*S*,*R*)-Pt2	792	0.292	-3.9	
(*S*,*R*,*S*)-Pt2	794	0.285	3.8	

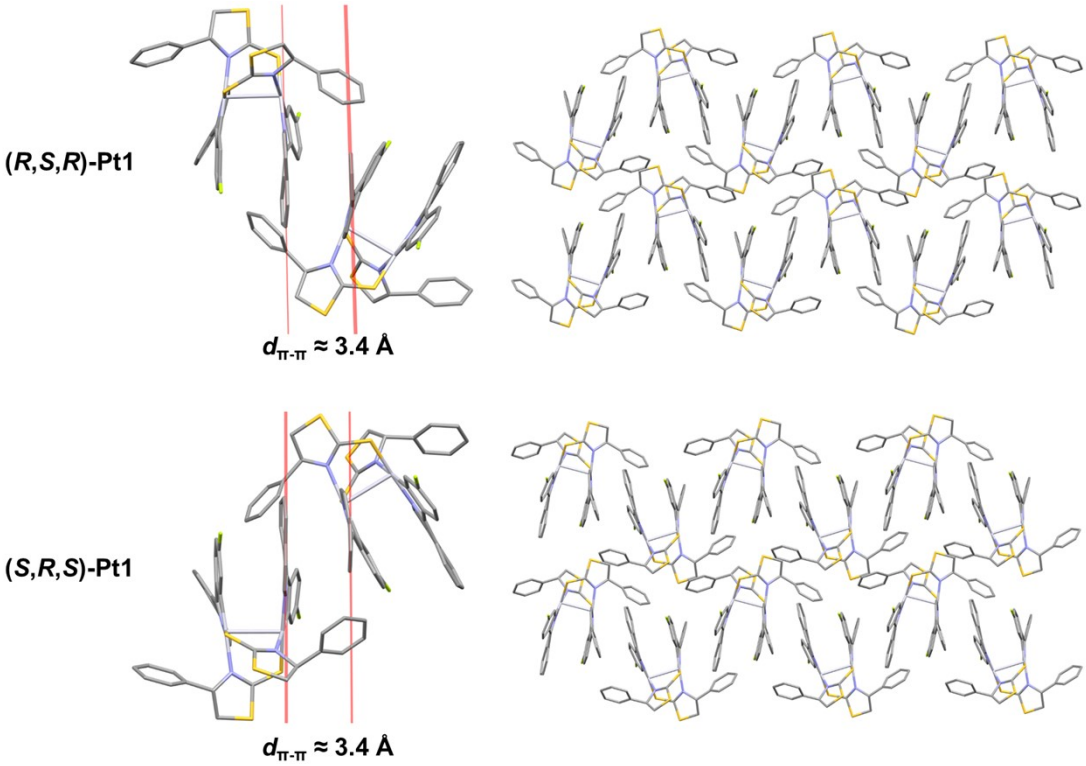

Figure S1. The molecular stacking and intermolecular $\pi\cdots\pi$ interactions between molecules in the crystals of **(*R*,*S*,*R*)/(*S*,*R*,*S*)-Pt1**.

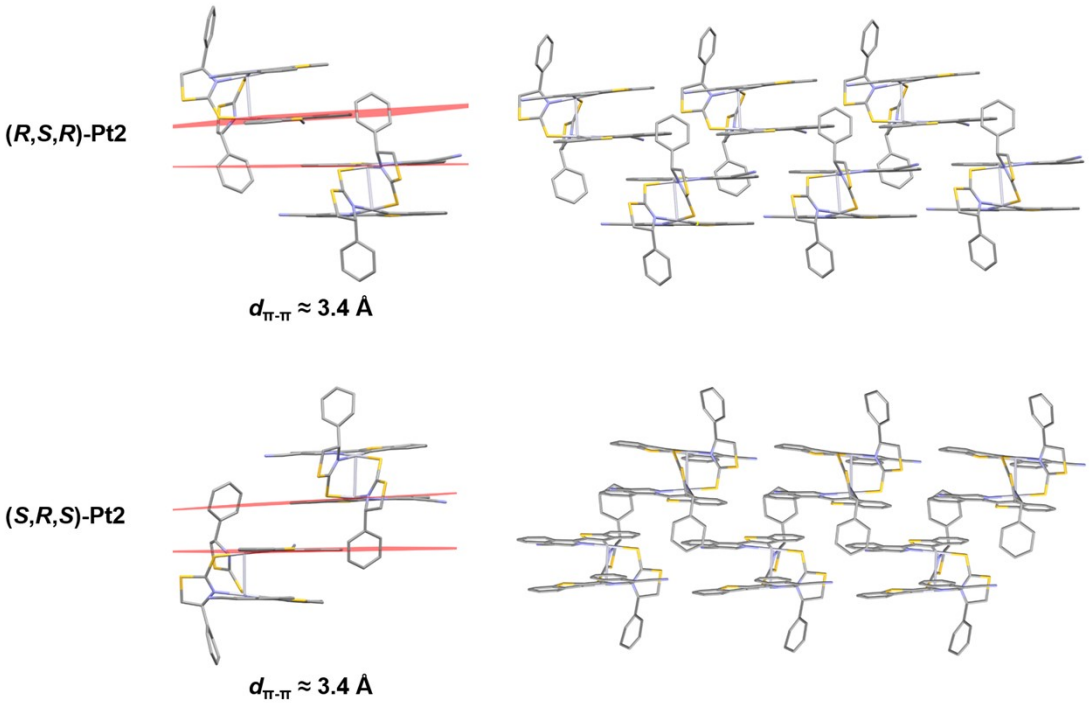

Figure S2. The molecular stacking and intermolecular $\pi\cdots\pi$ interactions between molecules in the crystals of **(*R*,*S*,*R*)/(*S*,*R*,*S*)-Pt2**.

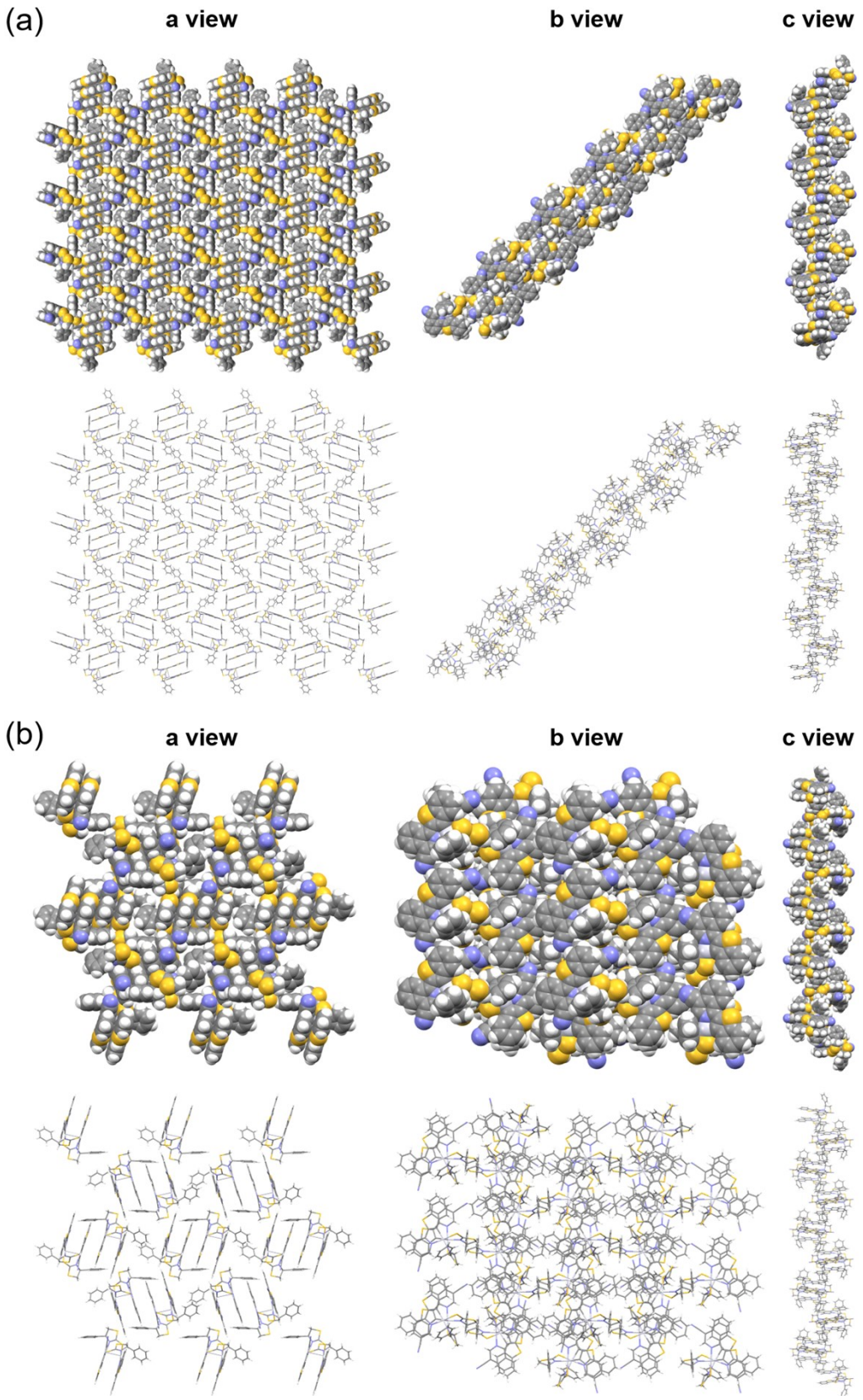

Figure S3. Molecular stacking in crystals of (a) **(*R*,*S*,*R*)-Pt2** and (b) **(*S*,*R*,*S*)-Pt2** with different view direction.

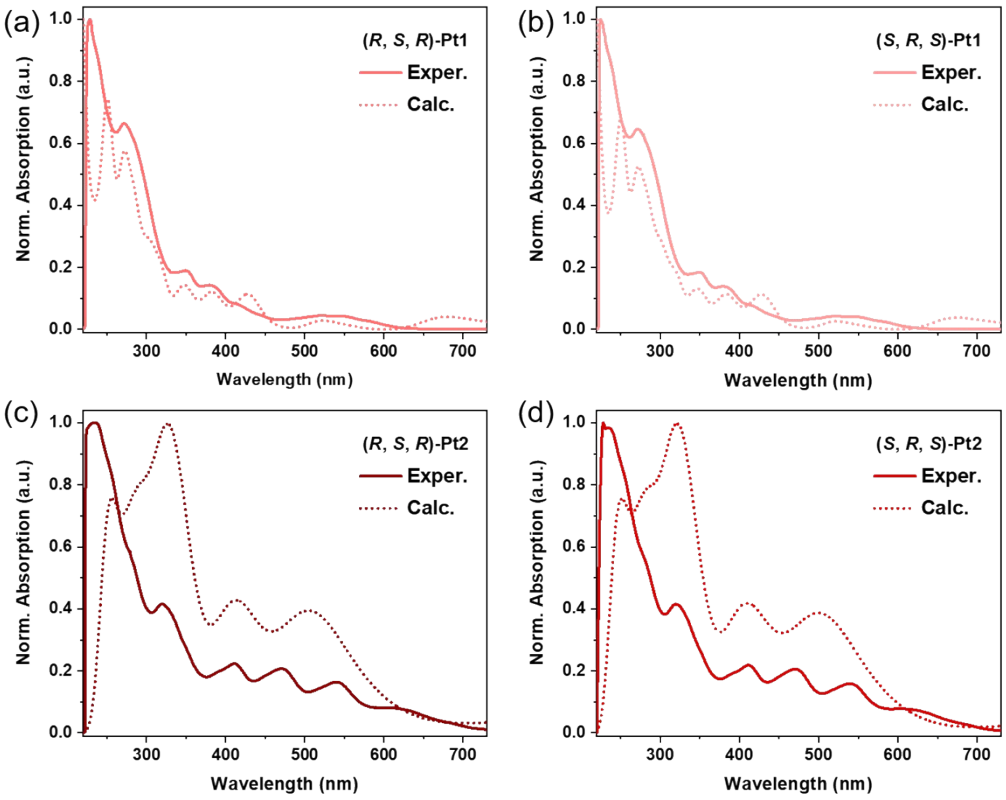

Figure S4. Experimental and calculated absorption spectra of Pt(II) complexes in CH_2Cl_2.

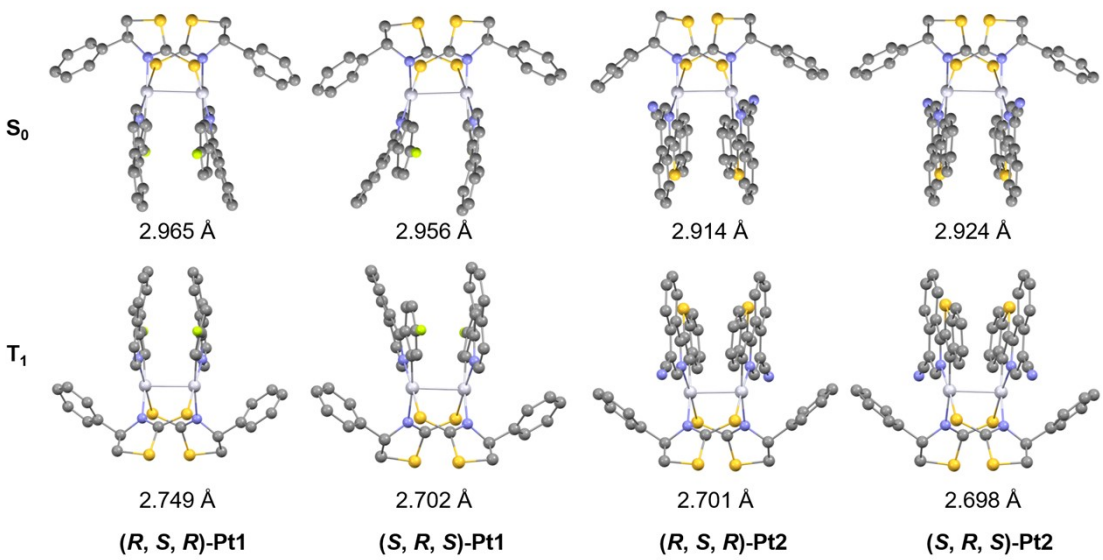

Figure S5. Optimized S_0 and T_1 geometries of Pt(II) complexes and their Pt-Pt distances.

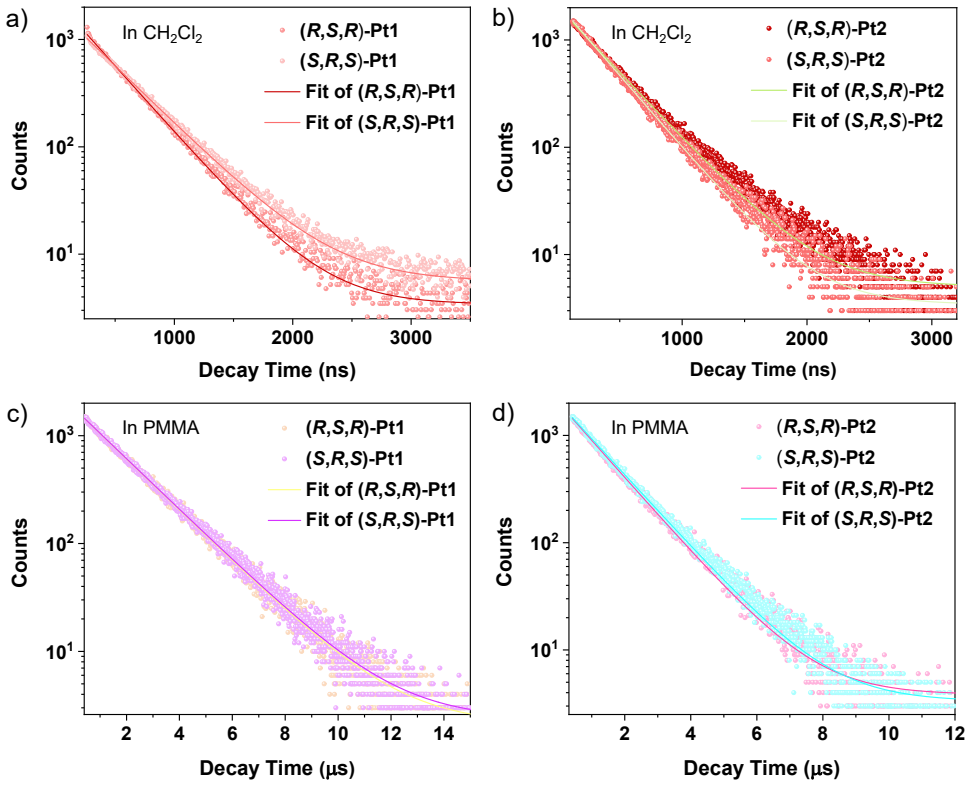

Figure **S6.** PL decay curves of Pt(II) complexes in degassed CH_2Cl_2 at 1×10^{-5} M (a,b) and 5 wt% PMMA film (c,d) at room temperature under the excitation of a 375 nm-laser.

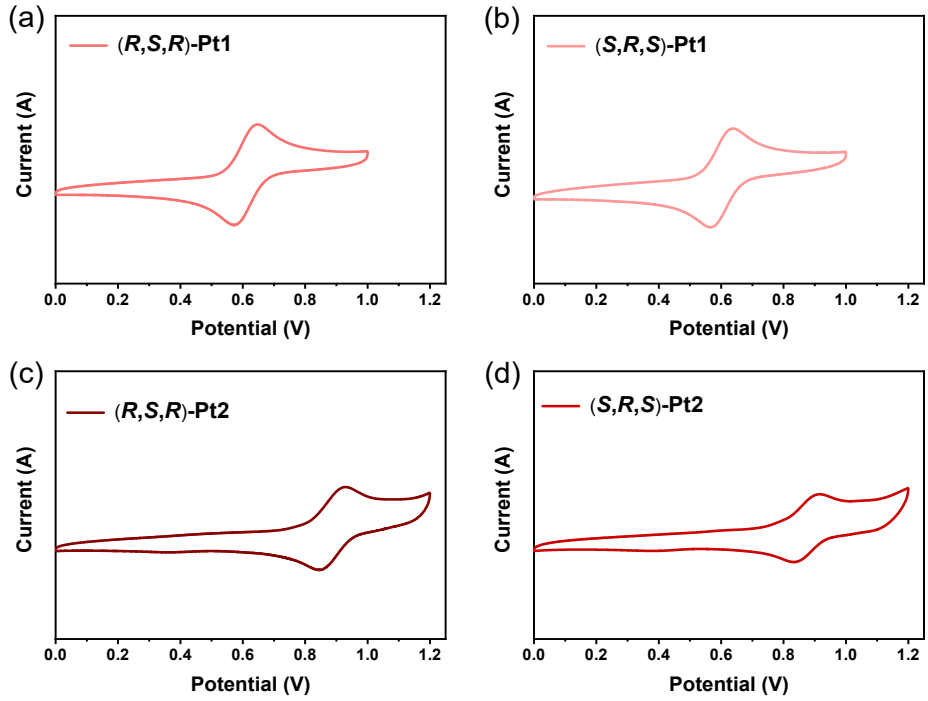

Figure S7. Cyclic voltammetry curves of Pt(II) complexes in CH_3CN with ferrocene as the internal standard under a scan rate of 100 mV/s.

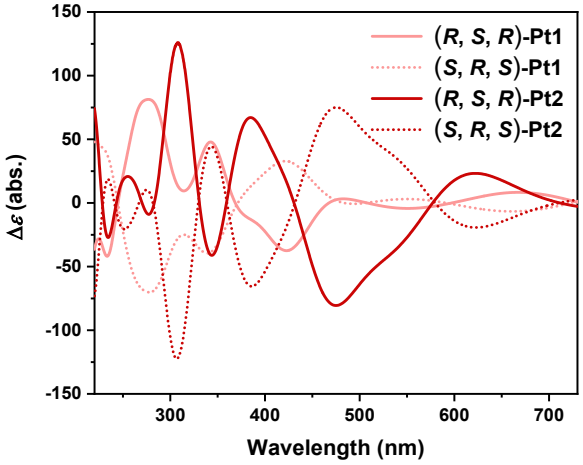

Figure S8. The calculated CD spectra for Pt(II) complexes.

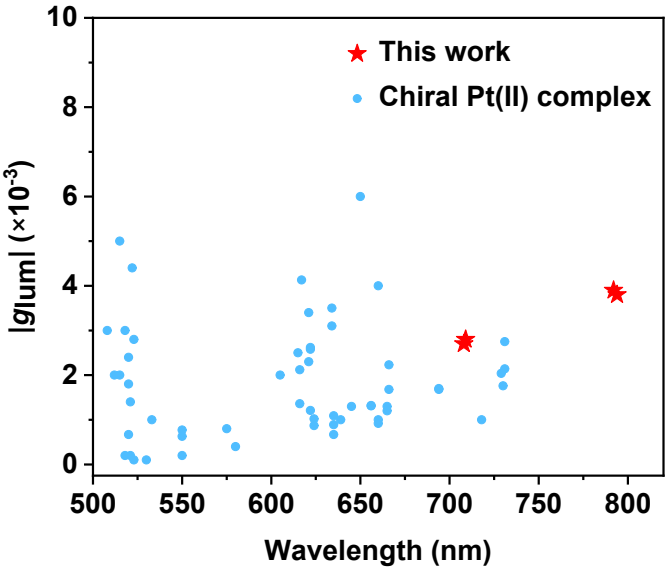

Figure S9. Comparison of g_{lum} of designed Pt(II) complexes with the reported chiral Pt(II) complexes.

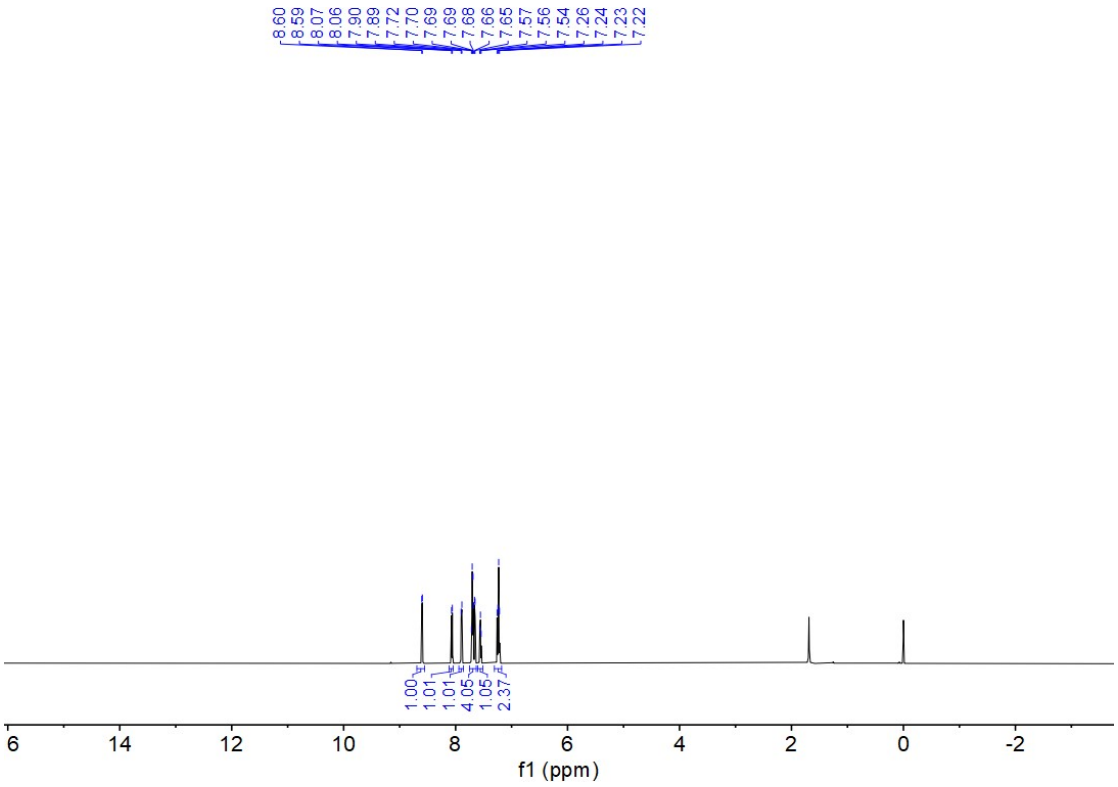

Figure S10. ^{1}H NMR spectrum for F-Hpiq in $CDCl_3$ at room temperature.

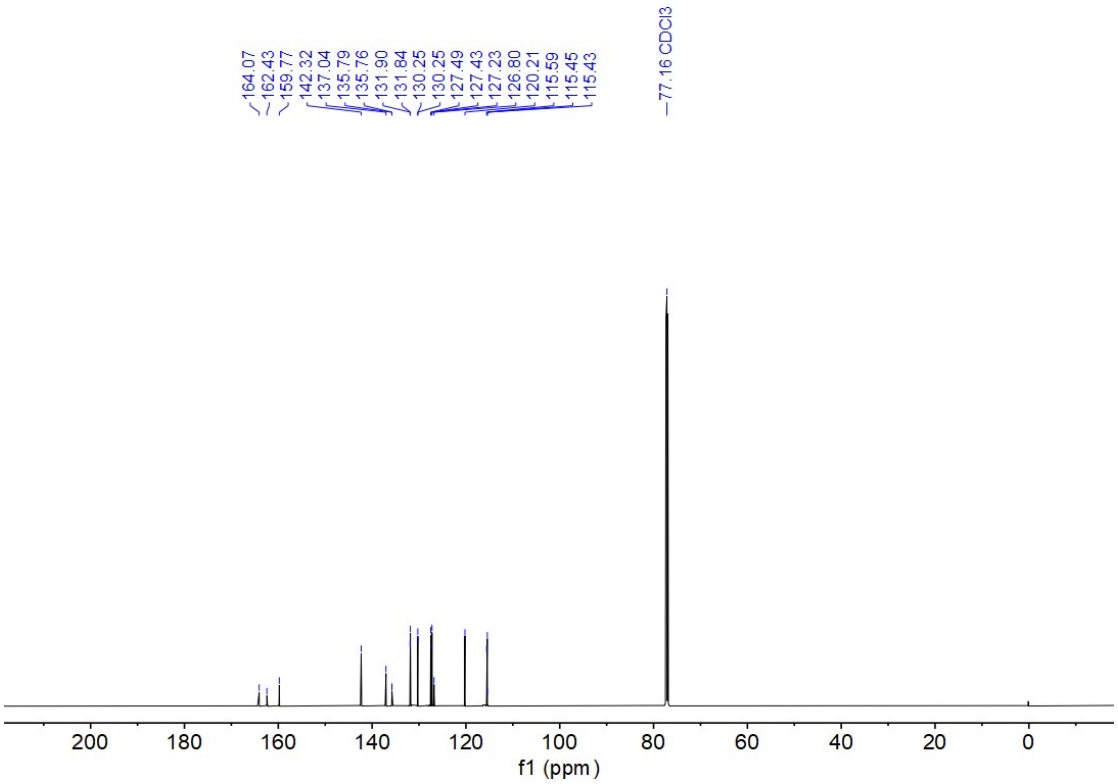

Figure S11. $^{13}C\{^{1}H\}$ NMR spectrum for F-Hpiq in $CDCl_3$ at room temperature.

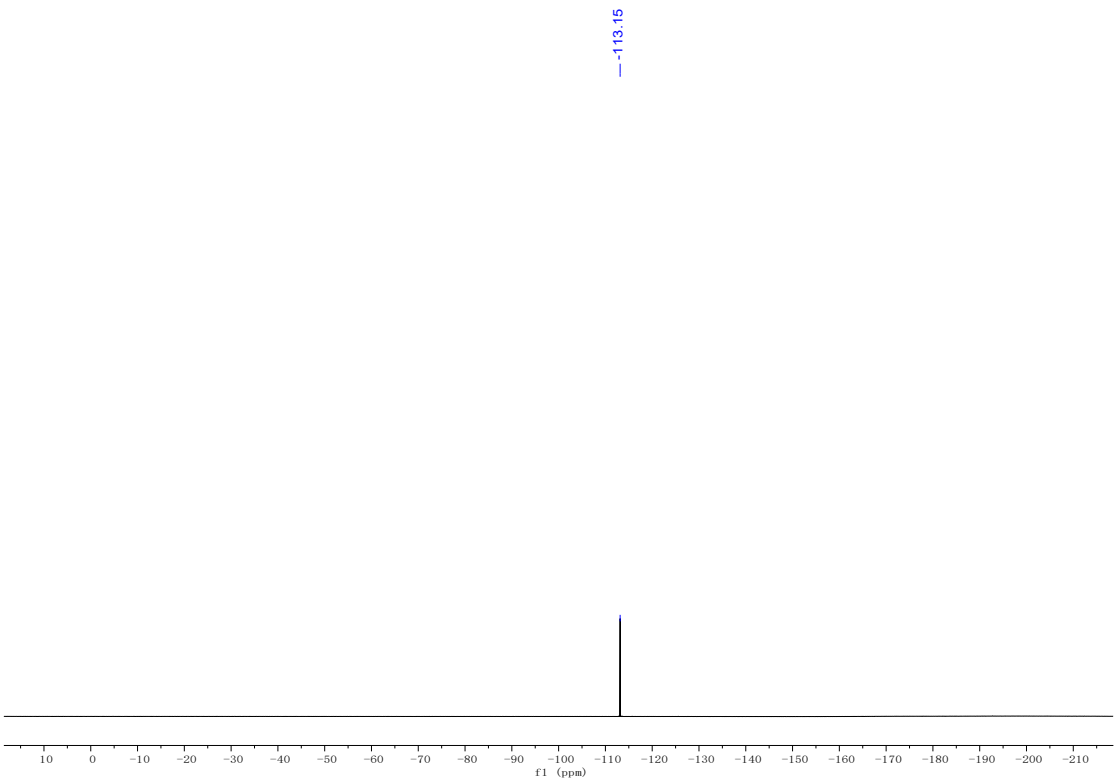

Figure S12. $^{19}F\{^{1}H\}$ NMR spectrum for F-Hpiq in $CDCl_3$ at room temperature.

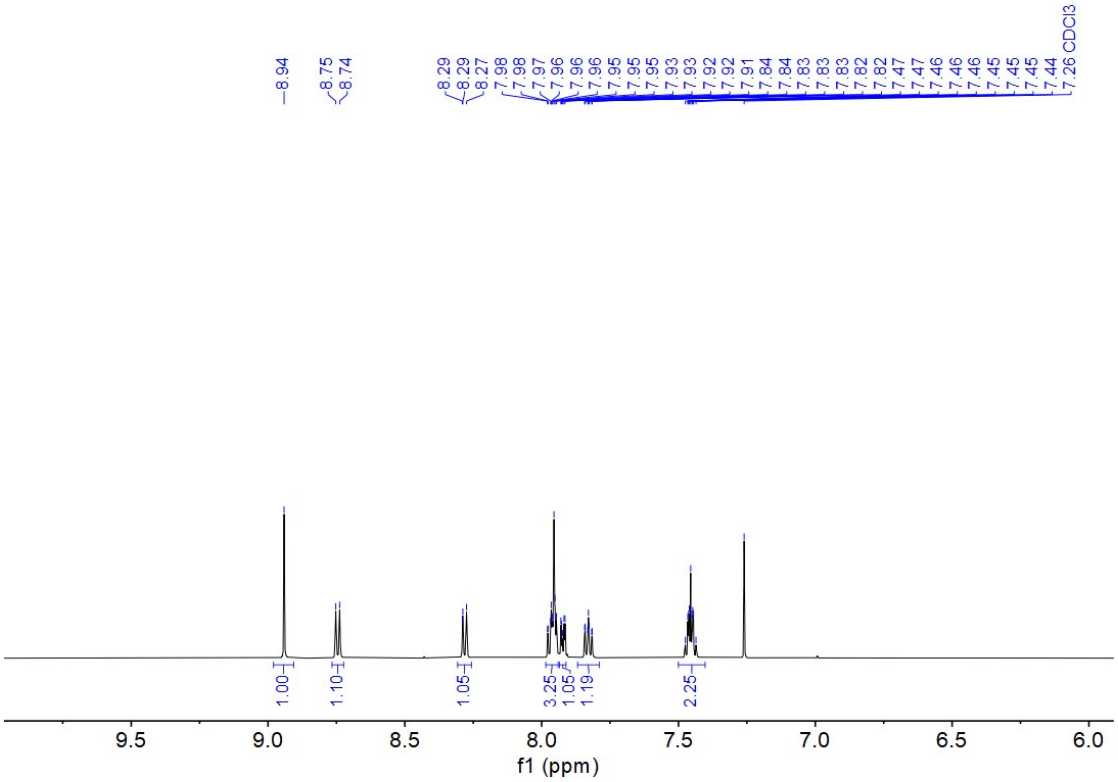

Figure S13. ^{1}H NMR spectrum for CN-Hiqbt in $CDCl_3$ at room temperature.

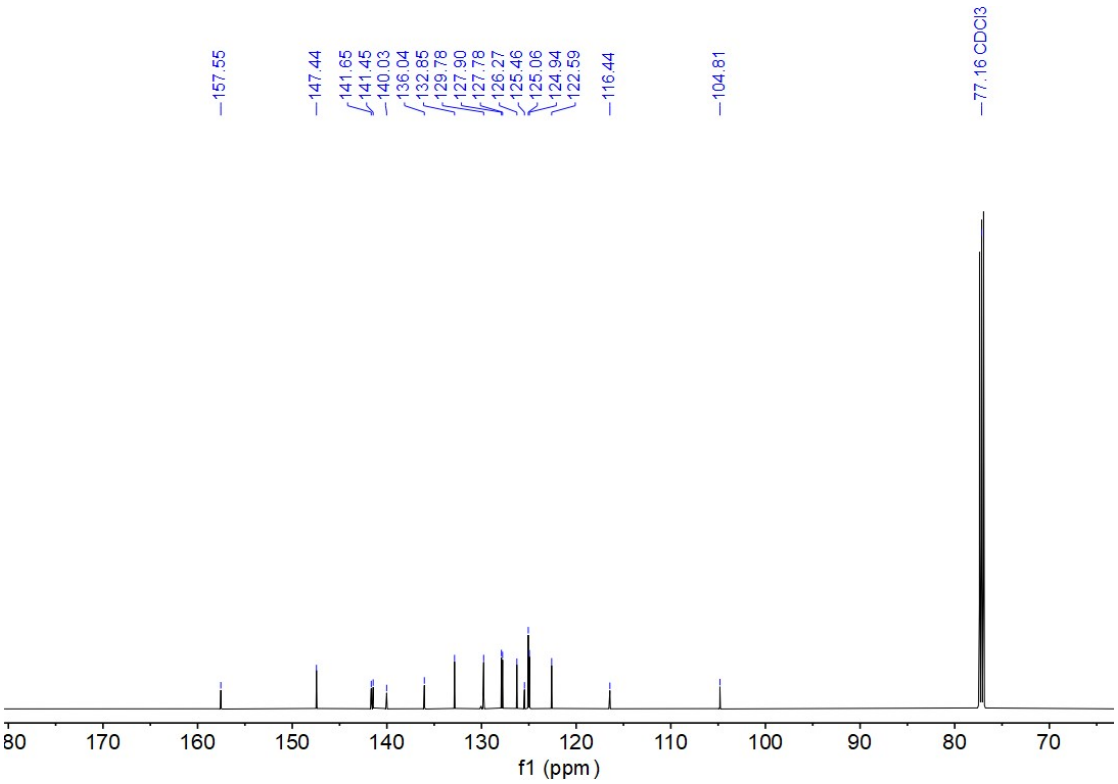

Figure S14. $^{13}C\{^{1}H\}$ NMR spectrum for CN-Hiqbt in $CDCl_3$ at room temperature.

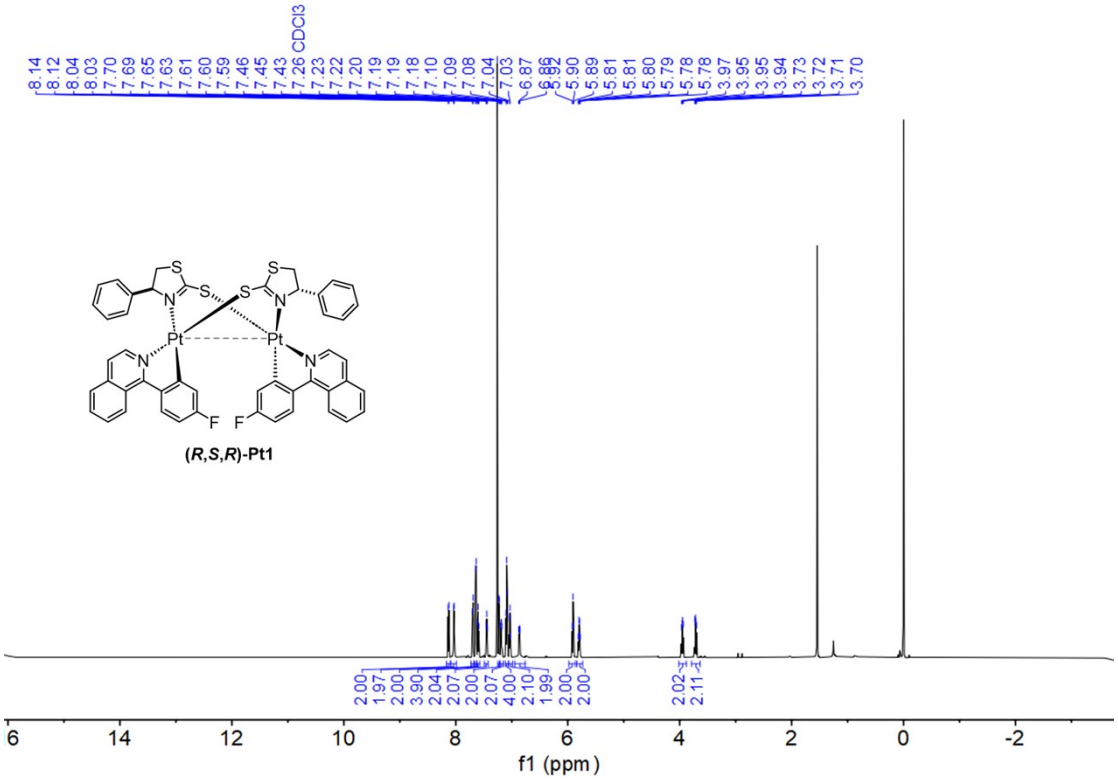

Figure S15. ^{1}H NMR spectrum for **(*R*,*S*,*R*)-Pt1** in $CDCl_3$ at room temperature.

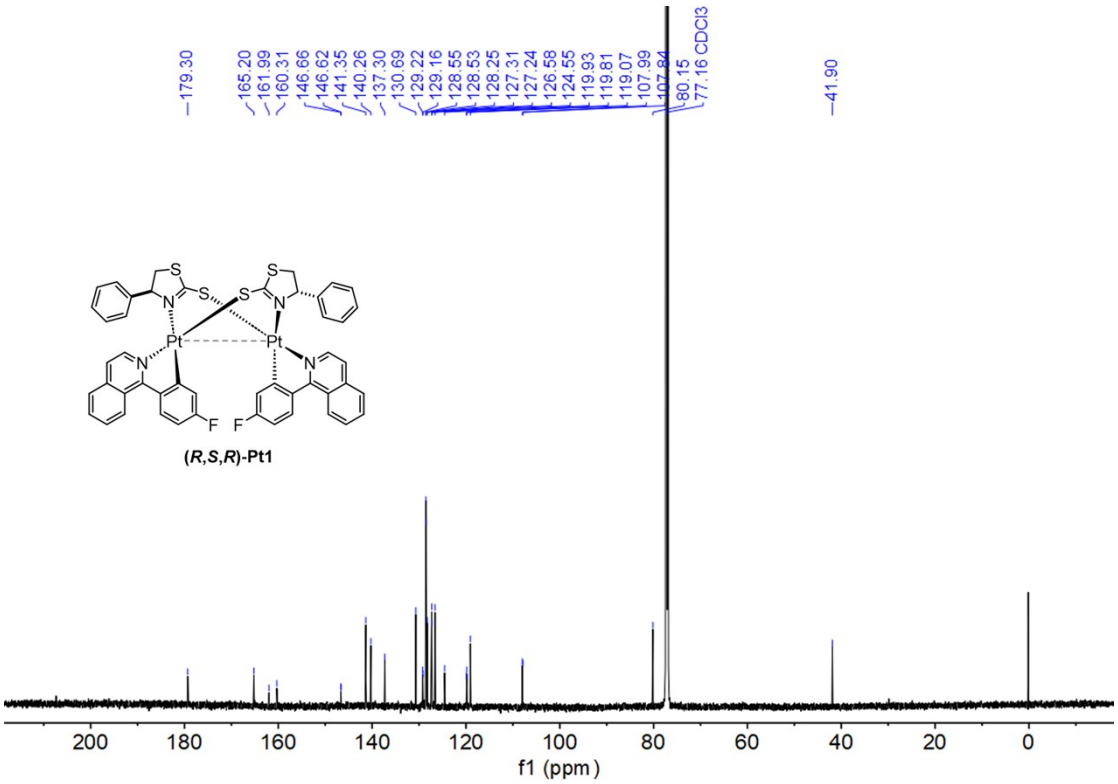

Figure S16. $^{13}C\{^{1}H\}$ NMR spectrum for **(*R*,*S*,*R*)-Pt1** in $CDCl_3$ at room temperature.

Figure S17. $^{19}F\{^{1}H\}$ NMR spectrum for **(*R*,*S*,*R*)-Pt1** in $CDCl_3$ at room temperature.

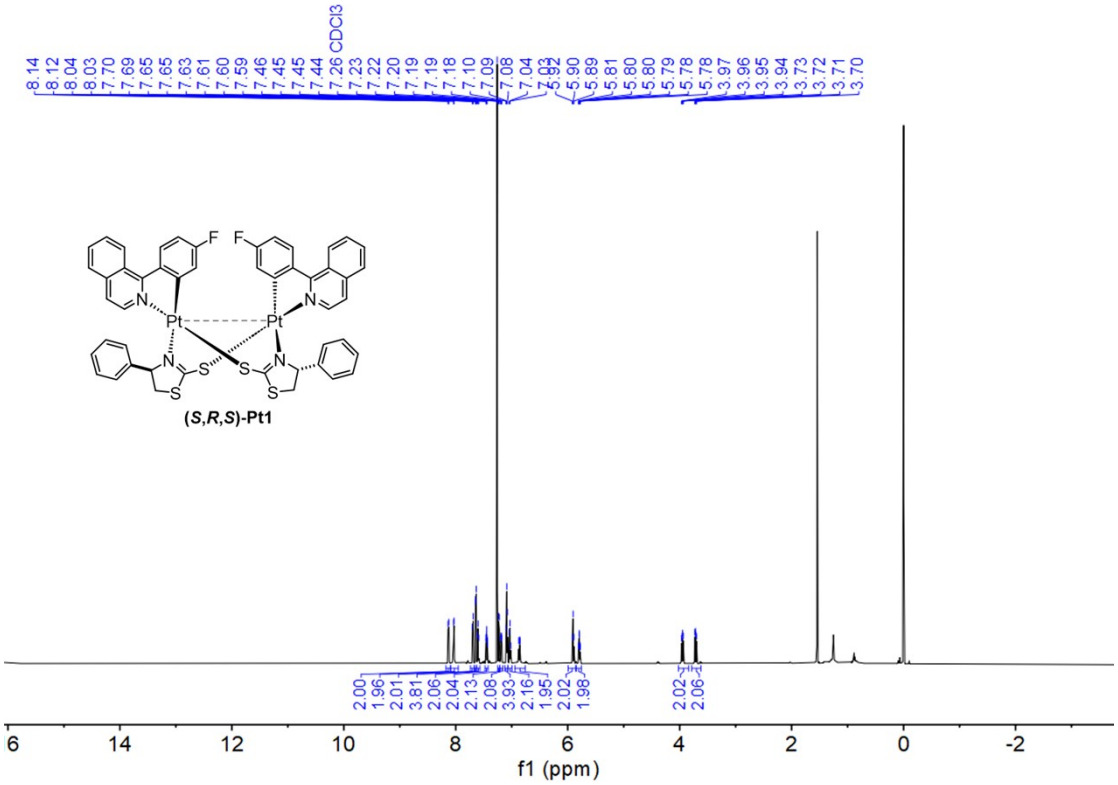

Figure S18. ^{1}H NMR spectrum for **(*S*,*R*,*S*)-Pt1** in $CDCl_3$ at room temperature.

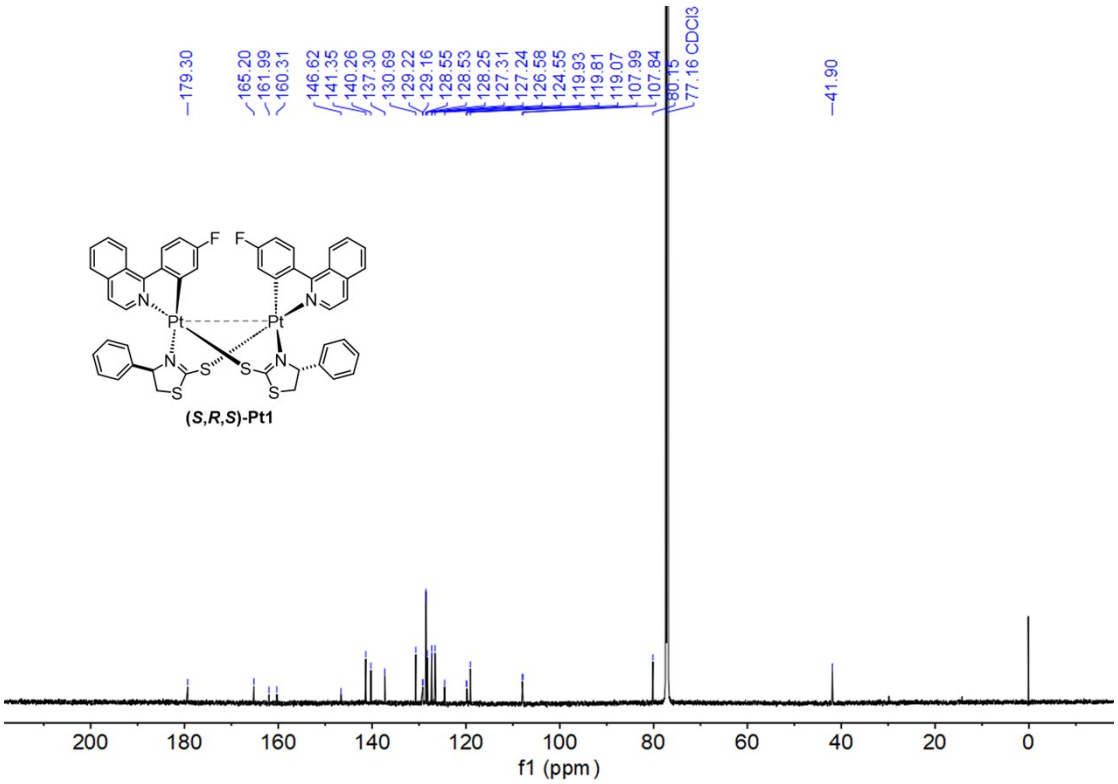

Figure S19. $^{13}C\{^{1}H\}$ NMR spectrum for **(*S*,*R*,*S*)-Pt1** in $CDCl_3$ at room temperature.

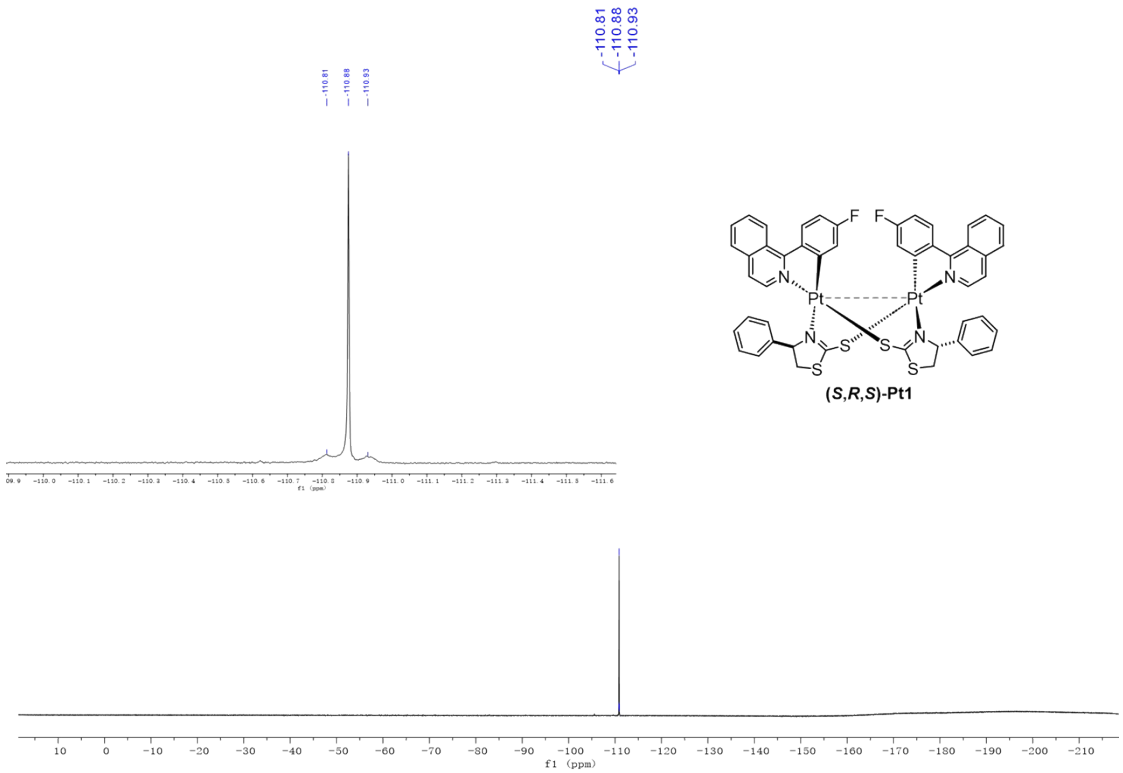

Figure S20. $^{19}F\{^{1}H\}$ NMR spectrum for **(*S*,*R*,*S*)-Pt1** in $CDCl_3$ at room temperature.

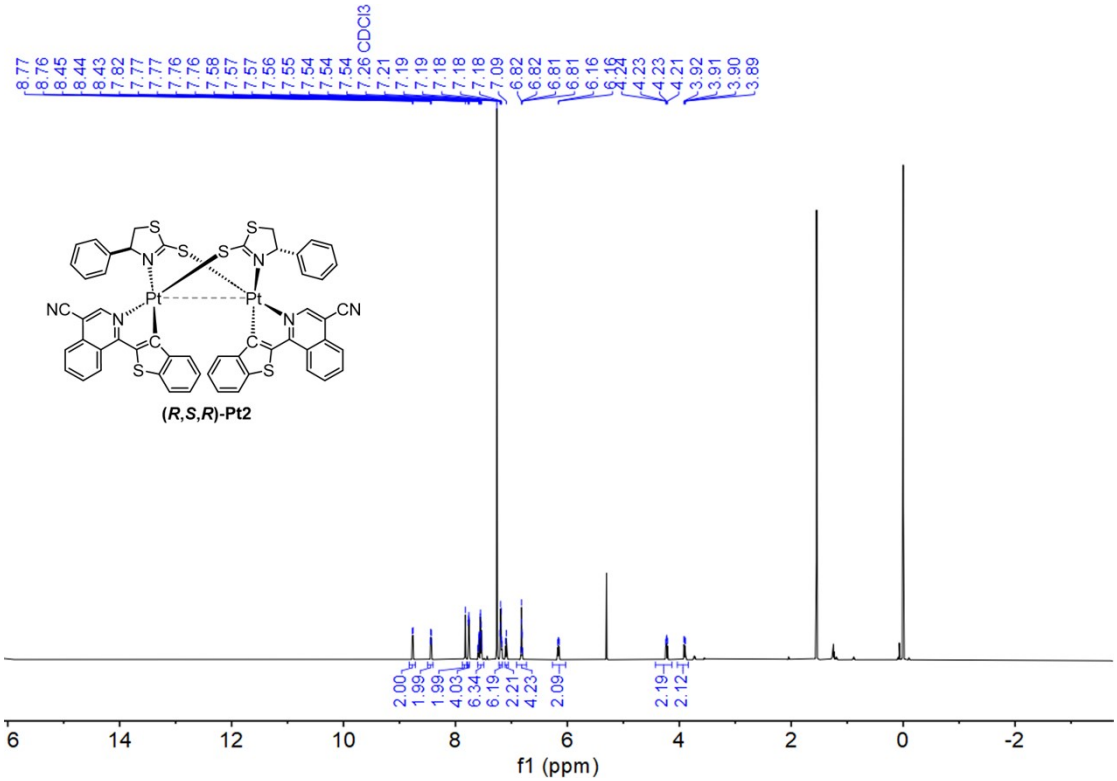

Figure S21. ^{1}H NMR spectrum for **(*R*,*S*,*R*)-Pt2** in $CDCl_3$ at room temperature.

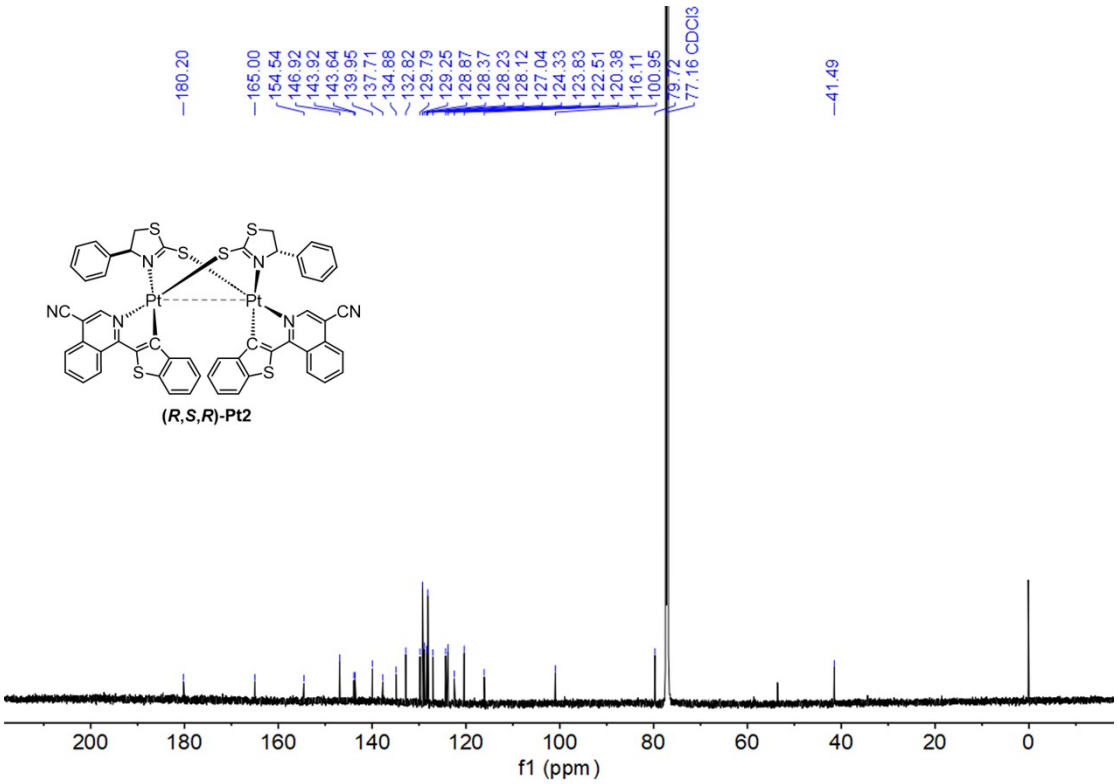

Figure S22. $^{13}C\{^{1}H\}$ NMR spectrum for **(*R*,*S*,*R*)-Pt2** in $CDCl_3$ at room temperature.

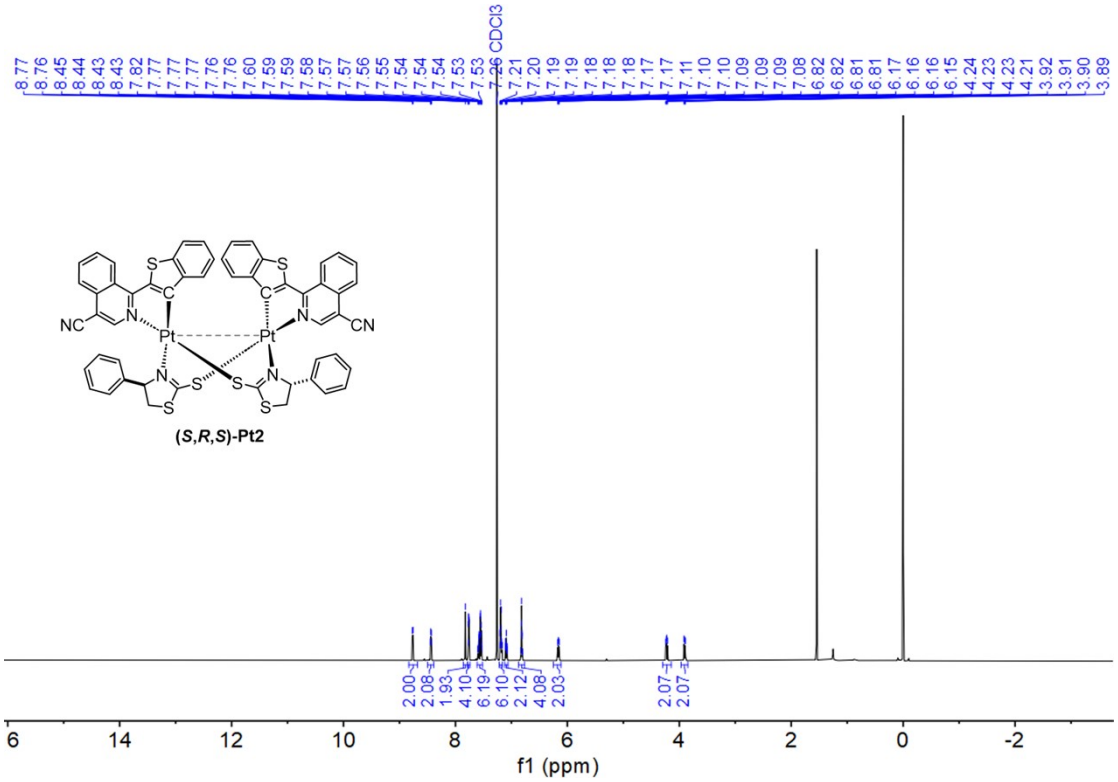

Figure S23. ^{1}H NMR spectrum for **(*S*,*R*,*S*)-Pt2** in $CDCl_3$ at room temperature.

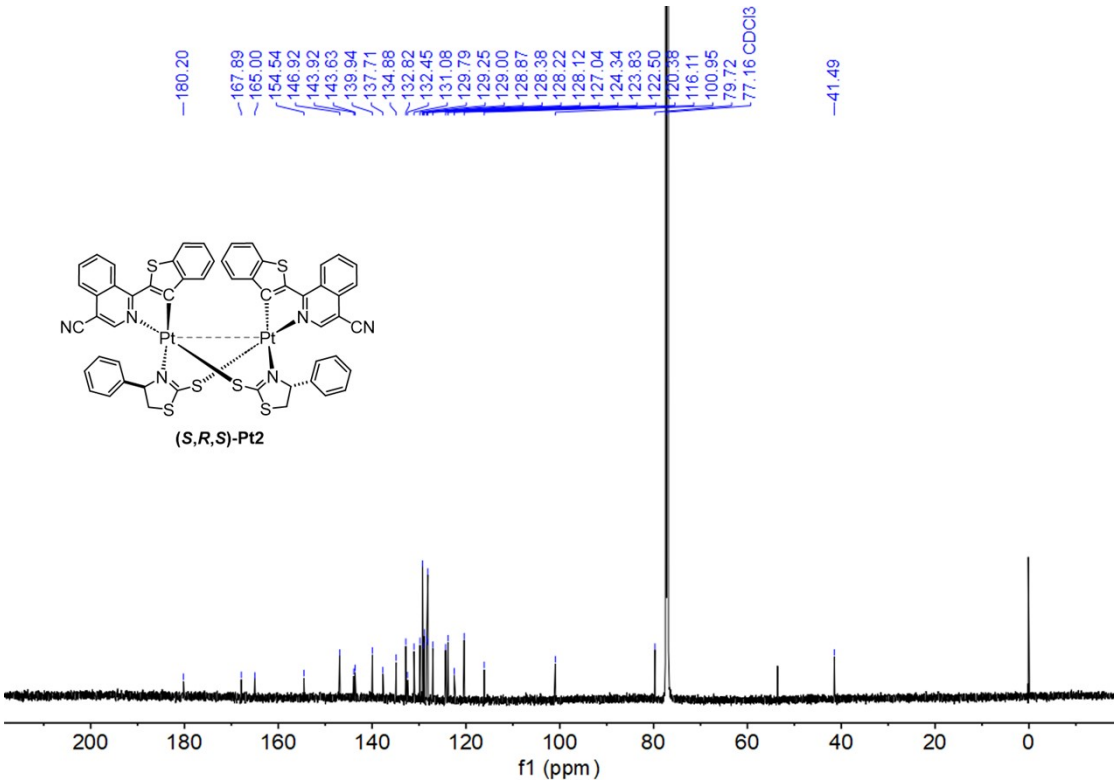

Figure S24. $^{13}C\{^{1}H\}$ NMR spectrum for **(*S*,*R*,*S*)-Pt2** in $CDCl_3$ at room temperature.

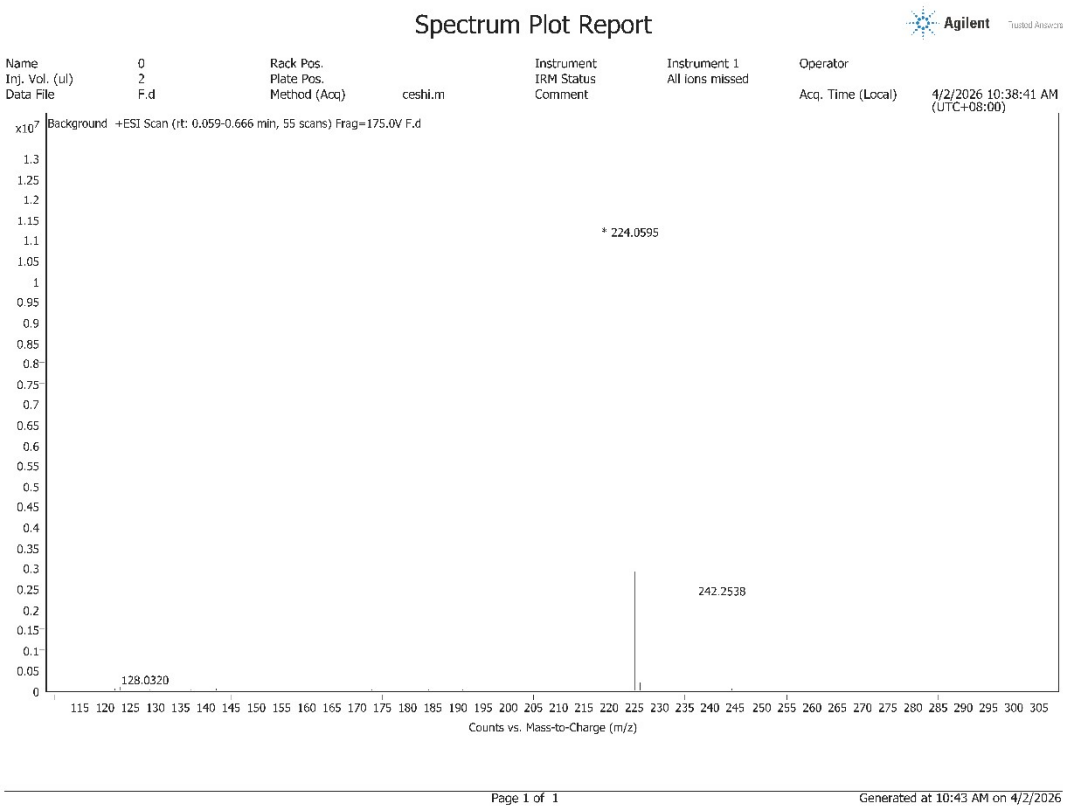

Figure S25. The mass spectrum for **F-Hpiq**.

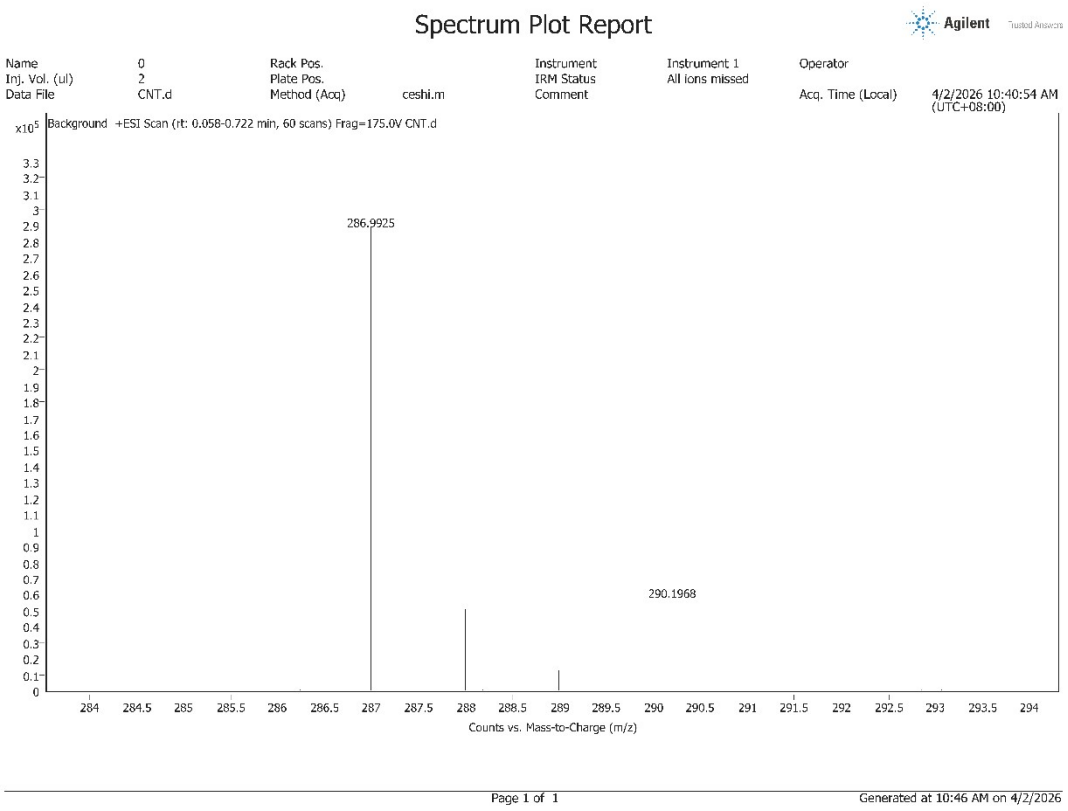

Figure S26. The mass spectrum for **CN-Hiqbt**.

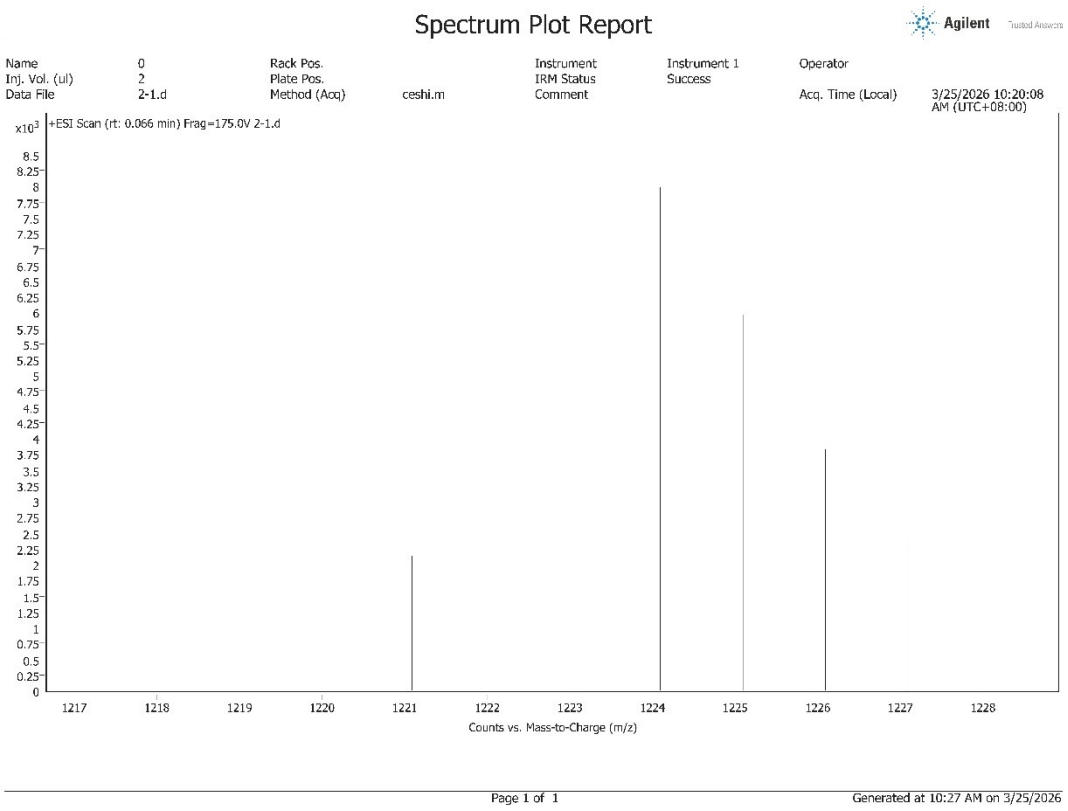

Figure S27. The mass spectrum for **(*R*,*S*,*R*)-Pt1**.

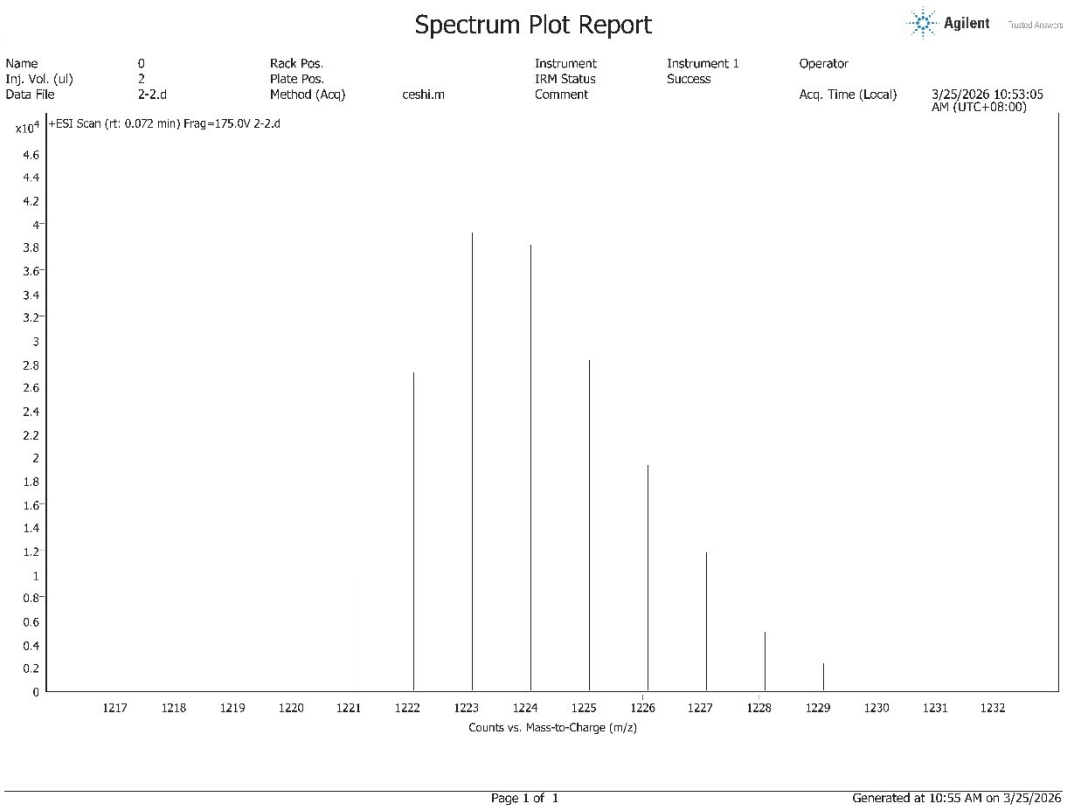

Figure S28. The mass spectrum for **(*S*,*R*,*S*)-Pt1**.

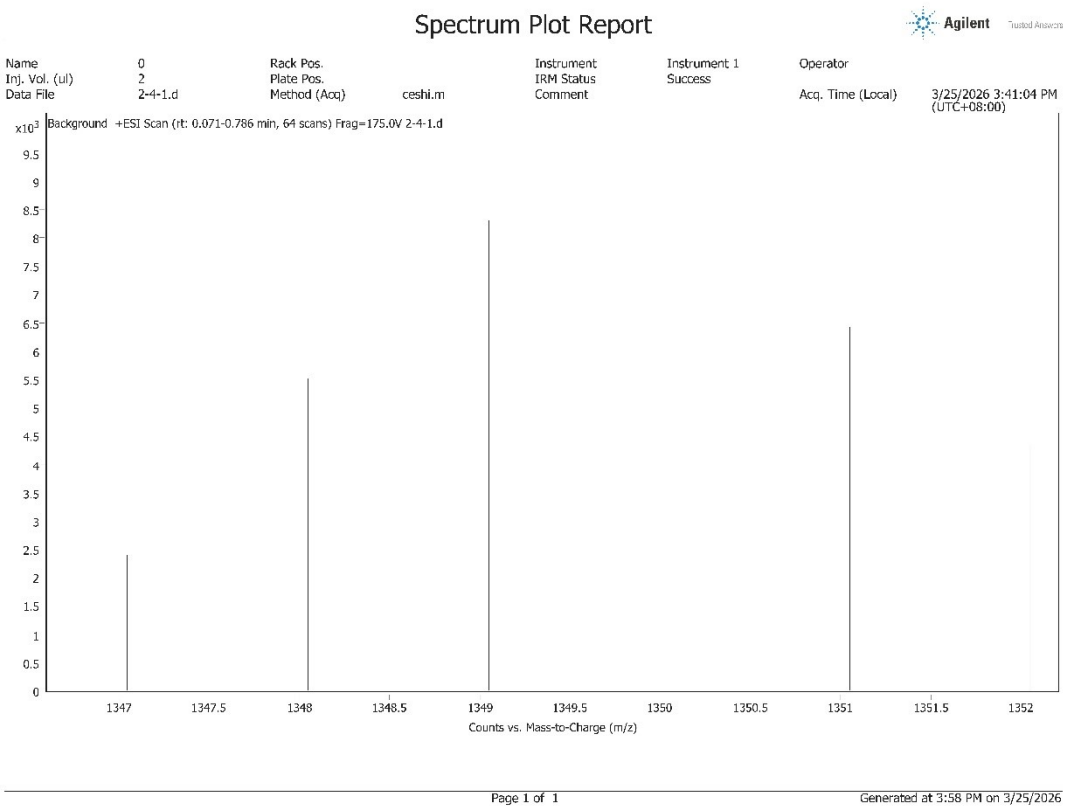

Figure S29. The mass spectrum for **(*R*,*S*,*R*)-Pt2**.

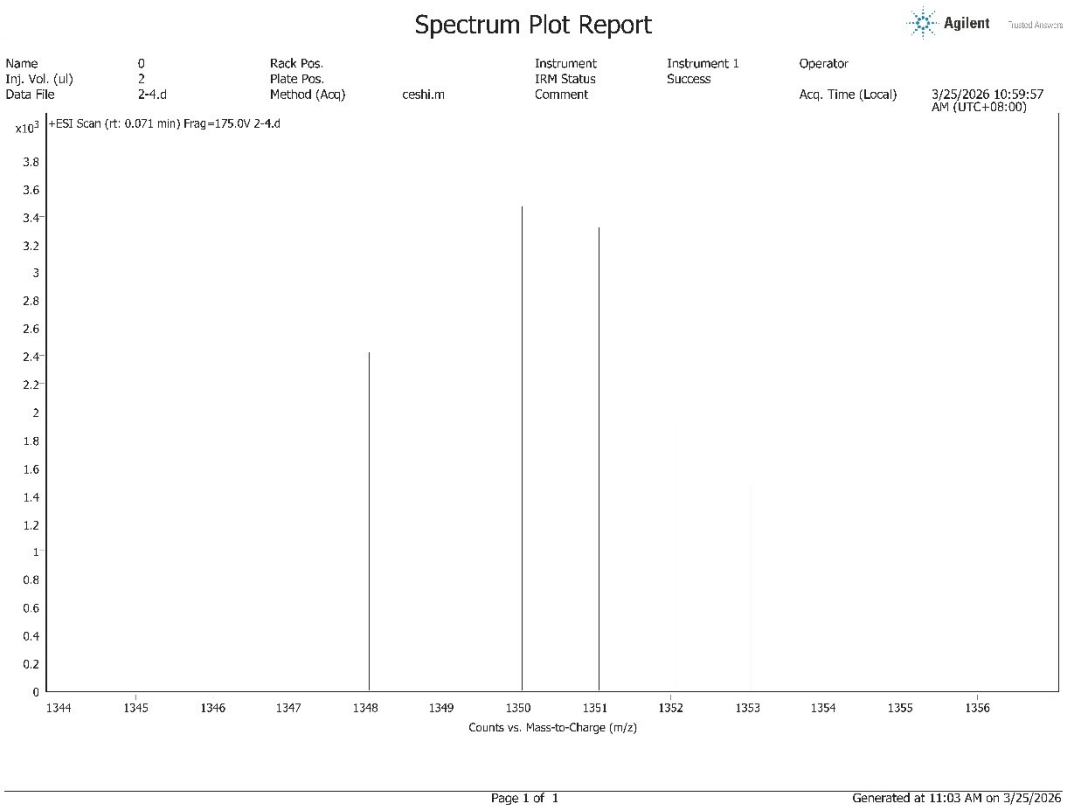

Figure S30. The mass spectrum for **(*S*,*R*,*S*)-Pt2**.

Supplementary References

(1) Sheldrick, G. M., A short history of SHELX. *Acta Crystallogr. Sect. A* **2008,** *64*, 112-122.

(2) Sheldrick, G. M., Crystal structure refinement with SHELXL. *Acta Crystallogr. Sect. C-Struct. Chem.* **2015,** *71*, 3-8.

(3) Lübben, J.; Wandtke, C. M.; Hübschle, C. B.; Ruf, M.; Sheldrick, G. M.; Dittrich, B., Aspherical scattering factors for SHELXL—model, implementation and application. *Acta Crystallogr. Sect. A* **2019,** *75*, 50-62.

(4) Zysman-Colman, E.; Ghosh, S. S.; Xie, G.; Varghese, S.; Chowdhury, M.; Sharma, N.; Cordes, D. B.; Slawin, A. M. Z.; Samuel, I. D. W., Solution-processable silicon phthalocyanines in electroluminescent and photovoltaic devices. *ACS Appl. Mater. Interfaces* **2016,** *8*, 9247-9253.

(5) Chen, H.-Y.; Chen, C.-T.; Chen, C.-T., Synthesis and characterization of a new series of blue fluorescent 2,6-linked 9,10-diphenylanthrylenephenylene copolymers and their application for polymer light-emitting diodes. *Macromolecules* **2010,** *43*, 3613-3623.

(6) Weigend, F.; Ahlrichs, R., Balanced basis sets of split valence, triple zeta valence and quadruple zeta valence quality for H to Rn: Design and assessment of accuracy. *Phys. Chem. Chem. Phys.* **2005,** *7*, 3297-3305.

(7) Weigend, F., Accurate Coulomb-fitting basis sets for H to Rn. *Phys. Chem. Chem. Phys.* **2006,** *8*, 1057-1065.

(8) Weigend, F., Hartree–Fock exchange fitting basis sets for H to Rn. *J. Comput. Chem.* **2008,** *29*, 167-175.

(9) Greenfield, J. L.; Wade, J.; Brandt, J. R.; Shi, X.; Penfold, T. J.; Fuchter, M. J., Pathways to increase the dissymmetry in the interaction of chiral light and chiral molecules. *Chem. Sci.* **2021,** *12*, 8589-8602.

(10) Wang, D.; Chen, X.; Yang, H.; Zhong, D.; Liu, B.; Yang, X.; Yue, L.; Zhou, G.; Ma, M.; Wu, Z., The synthesis of cyclometalated platinum(II) complexes with benzoaryl-pyridines as C^N ligands for investigating their photophysical, electrochemical and electroluminescent properties. *Dalton Trans.* **2020,** *49*, 15633-15645.